MOCVD Growth of Multifunctional III-Nitride Quantum Dots

Final Report

Agreement #: F49620-03-1-0294

Ian Ferguson, Professor
Matthew Kane and Shalini Gupta, Graduate Research Assistants
School of Electrical Engineering
Georgia Institute of Technology
Atlanta, Georgia 30332-250 U.S.A
Phone: 404-385-2885
Email: ianf@ece.gatech.edu

1. Overview

This is the final report for AFOSR Project #: F49620-03-1-0294 on the 'MOCVD Growth of Multifunctional III-Nitride Quantum Dots''. Significant progress was made in the course of this project, culminating the first evidence of ferromagnetism in MOCVD-grown $Ga_{1-x}TM_xN$ quantum dots (QDs). Furthermore tremendous progress has been made in the growth of bulk $Ga_{1-x}TM_xN$. Different transition metals were used to dope GaN at the bulk and the quantum level, to obtain a better understanding of the ferromagnetism mechanism in these materials. Two graduate students worked on this project researching the growth and the characterization of $Ga_{1-x}TM_xN$ based materials. In addition, this work has resulted in a book chapter, numerous papers and presentations and, as well as several invited talks. Listed below are the major accomplishments and outputs of this work; more details can be found within the text of this report.

Major Accomplishments:

- Provided evidence of ferromagnetism in alloyed $Ga_{1-x}TM_xN$ films grown by MOCVD
- Provided the first direct evidence of Mn-incorporation on the Ga lattice site in MOCVD-grown $Ga_{1-x}Mn_xN$ by EPR measurements
- Showed that ion implantation leads to secondary phase formation and incomplete damage recovery, providing further evidence for the need for homogeneous, device-quality dilute magnetic semiconductor growth methods such as MOCVD
- Demonstrated a strong correlation between the strength of the observed magnetic signal and the valence state of the Mn ions in $Ga_{1-x}Mn_xN$
- Produced $Ga_{1-x}Mn_xN$ light emitting diode structures with Mn containing active regions in one of the first device-related efforts in these materials
- Showed through magnetic property measurements evidence for possible formation of magnetic clusters, which can have significant ramifications on future device designs and the ultimate utility of this materials system.
- Showed Stranski-Krastanow like growth for GaN QDs.
- Demonstrated that by using growth conditions to control the size of the Quantum dot, the wavelength of light emitted can be changed to either blue or red shift due to quantum confinement or piezoelectric field.
- Showed that transition metal doping of GaN QDs enhances nucleation and reduces the size and increases the density of QDs.
- Showed hysteresis curves were obtained for both Mn and Fe doped GaN QDs.

2. Personnel and collaborations

Several persons are working under the direction of the PI. The two main graduate students working on this project are Matthew Kane and Shalini Gupta. Matthew has been focused on the growth and characterization of transition metal doped GaN. He has also been working on the growth of similar high crystal-quality single crystals of ZnO in order to find a common origin for room temperature ferromagnetism in these systems. Matthew has just defended his thesis and has accepted a position as an assistant professor beginning next fall. Shalini Gupta has been focused on the growth and characterization of transition metal doped nanostructures. She has just defended her Ph.D. proposal and will continue working on transition

metal doped nanostructures with an end goal of creating a spintronic device. In addition, Dr. Martin Strassburg, a post-doc fellow shared between Georgia State University and Georgia Tech has contributing significantly to this project process. He is an expert in optical characterization of wide bandgap semiconductors, and directed the optical characterization of these systems. In addition, he trained the newer graduate students on the photoluminescence measurements. Due to the interdisciplinary nature of the research group, over 15 other graduate students, undergraduates, and postdocs were exposed to the research and scientific methods employed in this study.

Because of the complicated nature of the materials system being studied here, several fruitful collaborations have been developed in order to maximize the usefulness of the research and the training involved. At Georgia Tech, collaborations have developed with Prof. Z. John Zhang's group in the school of chemistry and biochemistry. Prof. Zhang is an expert in ferromagnetism in solids, particular in nanoparticular systems and has provided useful guidance in the magnetic characterization of these systems. In the materials department, work has proceeded in collaboration with Prof. Christopher Summer's group, whose primary expertise lies in luminescent materials. In addition, Prof Summers served on Matthew Kane's thesis defense committee. In addition to these collaboration, efforts have also been developed with the group of Professor Samuel Graham in the School of Mechanical Engineering at Georgia Tech. This work has greatly enhanced the understanding of these materials through the use of specialized Raman spectroscopy measurements on these samples. Work has also taken advantage of the materials characterization tools available at Georgia State in Prof. Nikolaus Dietz group. Furthermore, because of the importance of the lattice environment on the behavior of the system and the complication of the variable valence in the transition metal elements, a collaboration has also developed with Prof. Wolfgang Gehlhoff and Dr. Axel Hoffmann at the Technical University in Berlin. This collaboration has enabled the direct observation of the manganese valence state through electron paramagnetic resonance measurements in the Mn-doped samples grown by MOCVD and additional access to more specialized spectroscopic measurement.

3. Mn Ion Implantation in GaN

In order to provide a baseline for the MOCVD-grown data, samples of varying initial doping levels were implanted in order to determine the effects of manganese introduction by a somewhat non-ideal method on the gallium nitride crystal. Also, because much of the initial work on the dilute magnetic system focused on using ion implantation as the source of the manganese in order to produce ferromagnetic semiconductor material. Previously, ion implantation has been found to lead to ferromagnetic behavior in this system. This work sought to elucidate the contributions from the magnetic ions via ion implantation. Samples were implanted with 3e16/cm^2 Mn^+ ions at an energy of 200 keV and a temperature of 400^{o}C in order to

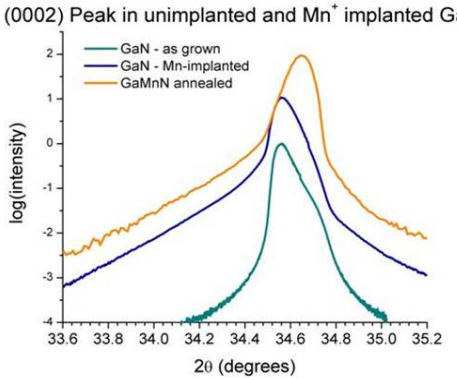

Figure 1: Peak shapes in as grown and implanted GaMnN samples. Note the low angle peak asymmetry and peak shift upon annealing.

promote dynamic annealing and to minimize the lattice damage. Various annealing procedures were studied in order to determine to recover the implantation damage. All annealing was performed face down on the GaN substrates in a flowing nitrogen atmosphere. X-ray diffraction was performed on the implanted samples both before and after annealing steps. In particular, reciprocal space mapping was used to analyze the symmetric reflections. Several key features were learned from these studies. Figure 1 shows a 2θ–ω scan of the (0002) reflection, compared with the sample before implantation. There is considerable peak asymmetry on the low angle side, as would be expected from the large tensile strain component in the lattice imparted by the initial implantation. Figure 1 also shows the effect of the annealing on the peak shape. When all scans are normalized to the sapphire (0006) position, it can be seen that there is a slight shift in the peak maximum to a higher angle; however, the low angle peak asymmetry remains even after significant annealing. These results indicate that at the high implantation concentrations, subsequent annealing is unable to incorporate sufficient nitrogen for the system to fully recover to a relaxed, dilute alloy. In addition, the highest temperature annealing procedure (900°C, 5 min) results in additional peaks appearing in the the x-ray diffraction scan which index to the impurity phase $Mn_6N_{2.58}$. In addition, a different impurity phase, $Mn_3GaN_{0.5}$, appeared in one implanted sample annealed at a lower temperature (700°C 5 min).

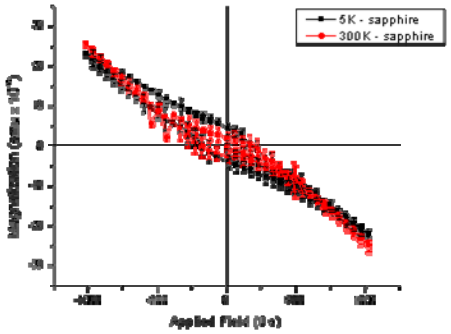

Figure 2: Magnetization curve from bare sapphire substrates. The residual area in the curve is attributed to Cr^{3+} contaminants in the substrate.

The magnetization behavior of this sample was studied via Squid magnetometry. In order to provide a baseline for these samples, a bare sapphire wafer was measured, as shown in Figure 2. The signal is predominantly diamagnetic at both 5 K and 300 K, as would be expected from the sapphire. There is, however, a slight area in the signal which is likely due to a magnetic impurity in the substrate The Cr^{3+} ruby transition is common in sapphire and is the likely source of this behavior. Next, the magnetic signature of the n-type implanted sample was measured, as shown in Figure 3. Hysteresis is observed in this sample at both room temperature and at 5K. The peak shape is somewhat unusual for the 5 K sample. Looking at the 5 K contribution of the sapphire substrate, it clear that this is the likely source of the signal variation, and provides a contribution on the order of that of the implanted GaN:Mn sample. Similar hysteresis curves were observed in implanted intrinsic and p-type samples. The major lessons learned from the implantation study so far are:

- The implanted samples retain significant interstitial lattice damage, even after significant annealing
- Overannealing the implanted samples results in phase separation of MnN and GaMn impurities

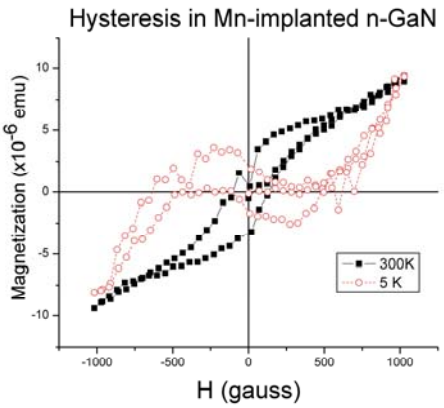

Figure 3: M vs H curve for Mn+ implanted n-GaN at 5 K and 300 K. At 5 K the background signal from the sapphire substrate is clearly evident.

- Ferromagnetic behavior can be observed in the implanted samples, regardless of the carrier type and concentration
- Chromium impurities in the substrate complicate the analysis of the magnetic behavior of these samples.

Similar findings have been reported for ion implanted samples in the literature. It is important to note that we have been able to duplicate these findings. It is also clear that a more optimal technique for the growth of these materials is required; hence our studies via MOCVD of this materials system are still applicable and important to the overall understanding of these materials.

4. MOCVD growth and structural properties of $Ga_{1-x}TM_xN$

Prior to the nanostructure growth thin films of $Ga_{1-x}TM_xN$ were grown to obtain a better a better understaning of the material growth chemistry and its bulk properties. To produce high quality material necessary for device implantation and possible spin injection studies, metalorganic chemical vapor deposition was used to grow nominally phase pure epilayers of $Ga_{1-x}Mn_xN$. The growth tool is shown in Figure 4.

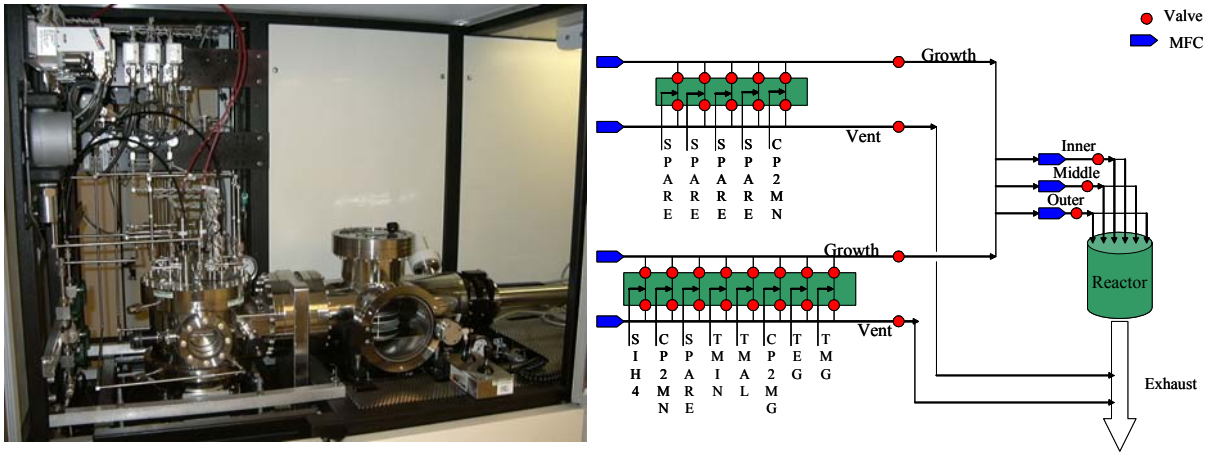

Figure 4: Photograph and gas flow of the MOCVD-growth tool. The system design is unique to the tool at Georgia Tech, and features dual path flow injection which prevents gas phase prereactions which could be detrimental to the growth of complicated transition metal doped GaN material.

It is important to recall the unique features of the growth tool available for this research as described in the previous reports [1] including a dual injector block, capability to rapidly switch the carrier gas, and a low temperature growth head. Using a standard hydrogen anneal, roughing, recover, and buffer layer technique, one micron thick virtual GaN templates were grown on c-cut sapphire substrates. Subsequently, individual layers of GaMnN were grown through the introduction of bis-cyclopentyldienyl manganese (Cp_2Mn) into the MOCVD reactor at the normal GaN growth temperature. Cp_2Mn is the manganese analog of the most common dopant used for p-type doping, Cp_2Mg, thus the chemistry was expected to be relatively similar to that used for the magnesium analog. A similar source was used for Fe doping. The vapor pressure of this compound, however, is relatively low compared to the trimethyl gallium used for

the gallium source, such that the optimal lattice concentrations could only be achieved by using low growth rates (~0.2 μm/hr). A modification was made to the reactor including a much larger mass flow controller for the Mn to allow for incorporation of greater concentrations of the transition metal dopant.

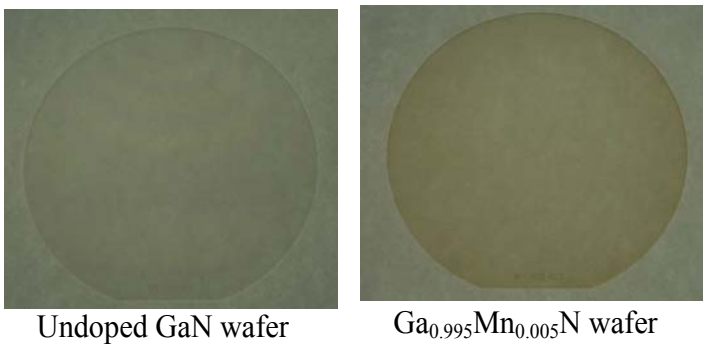

Undoped GaN wafer $Ga_{0.995}Mn_{0.005}N$ wafer

Figure 5: 2-inch wafers of GaN and GaMnN produced for this project. These reddish-colored wafers are the first MOCVD-grown GaMnN wafers of production size that exhibit ferromagnetism.

The as-grown films were specular in nature, as shown in the photograph of both the as-grown doped and undoped wafers in Figure 5. The films are reddish in color, which is consistent with films grown by other methods and is consistent with the behavior of interatomic transitions in ZnO:Mn, which should have similar crystal field parameters as GaN.

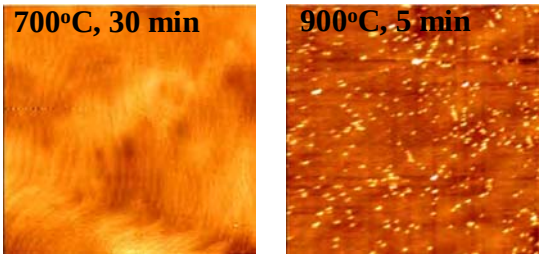

Figure 6: AFM of $Ga_{1-x}Mn_xN$ (x = 0.015) samples annealed at 700°C and 900°C for 30 and 5 minutes respectively.

Annealing studies performed on $Ga_{1-x}Mn_xN$ reveal that there is little change in the morphology of the layer with low temperature annealing (700°C) as seen in the Atomic Force Microscopy (AFM) image shown in Figure 6. However, an AFM image of the uncapped sample annealed at 900°C shows clear areas of what is likely second phase precipitate on the surface (Figure 6). These spots which indicate secondary phases that mostly likely occur at the nucleation sites were also apparent in samples annealed at 800°C. XRD scans can attribute this phase to either MnN or Mn_3GaN type phases. On the other hand, the annealed capped samples show no change in surface morphology even at elevated temperatures. This suggests that the primary mechanism for the decay of the thermodynamically unstable $Ga_{1-x}Mn_xN$ compound is through nitrogen desorption and phase rearrangement of the surface at the $Ga_{1-x}Mn_xN$-to-atmosphere interface in the absence of a reactive nitrogen environment that is present during MBE or MOCVD growth [2]. Annealing studies have yet to be carried out on $Ga_{1-x}Fe_xN$ samples.

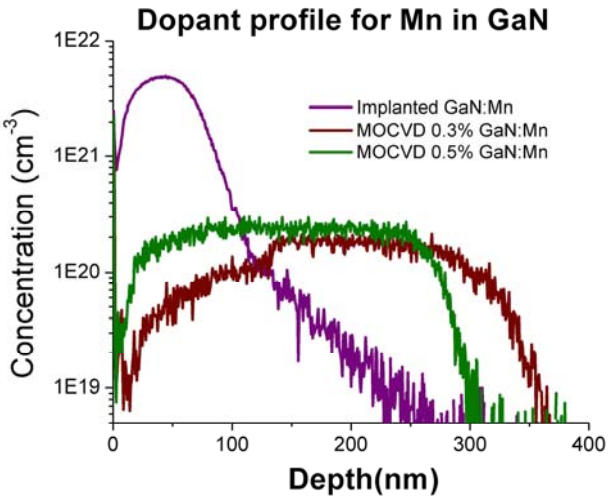

Figure 7: Secondary ion mass spectrometry of two of the as-grown MOCVD layers and an implanted layer. Note the uniform distribution of Mn in the as-grown layers.

In order to verify the level of incorporation of Mn into the layer, secondary ion mass spectrometry was

performed. Figure 7 shows the SIMS spectrum for one of the implanted as well as two of the MOCVD grown GaMnN samples. The implanted profile showed a peak shape expected from the elastic recoil of the implanted ions. On the other hand, the SIMS profile of the two MOCVD-grown layers is uniform throughout the depth of the two layers (250 nm and 300 nm). From integration of the implanted peak profile, it was found that the concentration of Mn in the two layers was 0.3% and 0.5% respectively. In the more heavily doped thicker layers, the concentration of Mn was found to be 0.8%. From these results, it appears that MOCVD provides a suitable method for the uniform introduction of transition metal into the layers.

High resolution X-ray diffraction analysis was performed in order to determine the quality and phase purity of the structures. A 2θ–ω scan is shown in Figure 8; on the same scale for comparison is shown a scan for undoped GaN. From this graph, it can be seen that the undoped and Mn-doped samples are very similar. Contrary to what is seen in the implanted sample, the GaN (0002) peak is symmetric and of similar FWHM to the as-grown undoped sample, indicating good incorporation of Mn-into the lattice without significant defect introduction and lattice damage as seen in the implanted sample. Figure 9 shows a reciprocal space map of the implanted sample, and undoped sample, and the MOCVD-grown sample. The MOCVD and undoped samples both show narrow, symmetric peaks, whereas the RSM of the implanted sample is much broader, with an asymmetric protrusion on the low angle side (towards the reciprocal lattice origin). This would be expected from the residual interstitial cations introduced into the lattice during the implantation which is not fully recovered in the anneal. The phase purity of the MOCVD-grown material is important to determine as well, as there are a number of ferromagnetic phases which contribute to or confuse the nature of the ferromagnetic origin in the signal. All of the phases have major peaks in the region scanned in Figure 8, and it is evident that no second phases are visible, contrary to what has been observed in samples grown by non-optimal MBE conditions or as shown above for our implanted samples. One interesting thing to note is that in the in the Mn-doped samples, peaks are visible in the 2θ–ω scan that index to the forbidden reflections (0001), (0003), and (0005) that are not seen in the undoped material, as seen in Figure 9.

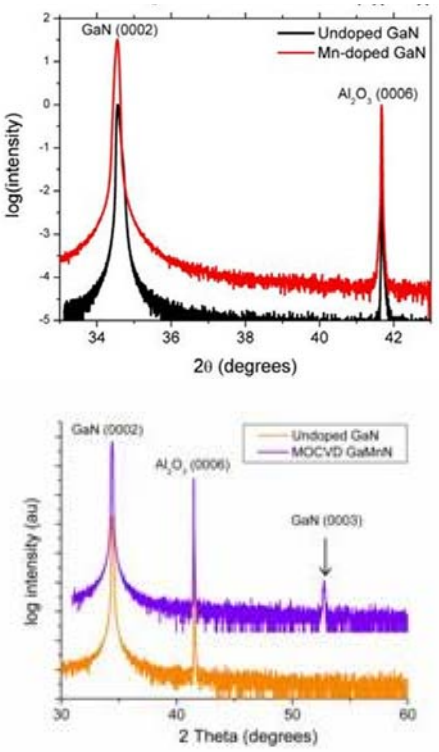

Figure 8: (left) HRXRD scan near GaN (0002) and sapphire (0006) peaks. Note that no other peaks are present due to second phases (top) 2θ–ω scan over broader range. In the Mn-alloyed samples, 'forbidden' (bottom) peaks are visible due to structural inhomogeneities.

Similar behavior has been observed previously in heavily-doped AlGaN [3] and in diffusion-grown GaMnN.[4] The peaks are indicative that the material quality may not be necessarily ideal, resulting in heavy compensation and/or long range ordering effects may be present.

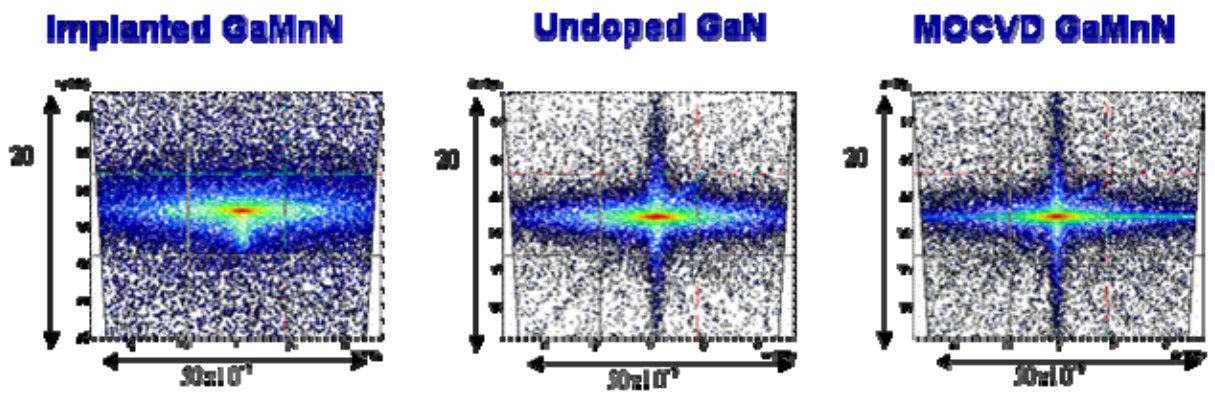

Figure 9: Reciprocal Space Maps (logarithmic contours) of the (0002) peak in GaN and implanted and MOCVD-grown GaMnN. The implanted scan shows a much broader peak with a low angle peninsula, whereas the MOCVD and undoped samples show very similar slopes.

5. Magnetic properties of MOCVD-grown $Ga_{1-x}Mn_xN$

Of critical importance to this work is the determination of the macroscopic ferromagnetic behavior. Whereas this is not necessarily an indication that the material is indeed a ferromagnetic diluted magnetic semiconductor, it is a necessary condition. In fact, there is still disagreement to this day on the nature of the ferromagnetism in this material system by all growth methods. In order to ascertain whether this material does exhibit ferromagnetic behavior, SQUID magnetometry was employed on the thickest, most heavily doped sample grown (to ensure the maximum contribution to the magnetic signal) to date. These results are shown in Figure 10. In this plot of magnetization versus applied field, clear hysteresis is observed in the signal. By taking the value of the saturation magnetization, the estimate film volume, and measured film concentration, it is possible to determine the average contribution of each Mn to the magnetic signal. In this case, we observe a value of 3.05 μ_B/Mn, which compares quite similarly to the lightly-doped samples grown by other techniques [5] but is extremely sensitive to errors in composition. Our work has demonstrated that ferromagnetic $Ga_{1-x}Mn_xN$ can be grown by in-situ incorporation by MOCVD, which has not been reported in the literature prior to the start of our work.

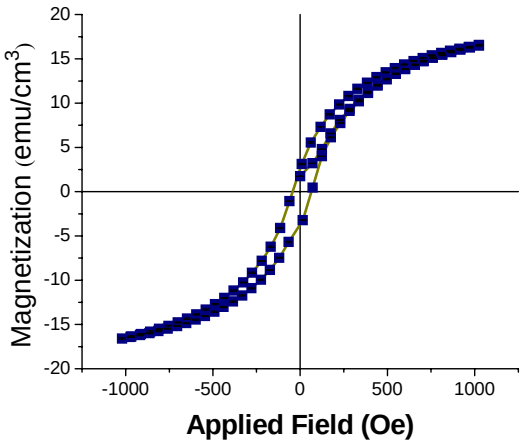

Figure 10: Room temperature hysteresis curve as measured in MOCVD-grown GaMnN (x=0.008).

An interesting behavior is observed with the addition of Mg and Si codopants into the material during the course of the growth process. Initially, this was done to explore the role of

carriers on the observed magnetic behavior. As seen in Figure 11, upon annealing, the magnetization of the same sample drops precipitously. There is still some area remaining in the hysteresis loop observed in this sample, indicating that the ferromagnetic phase is not completely lost or there may be a small contribution from local areas of the alloy that were unaffected by the anneal or that consist of ferromagnetic second phases. A close inspection of the zero-field cooled versus field-curves temperature dependent magnetization curves at the highest doping levels indeed shows a small irreversibility. This irreversibility has been used on several occasions to estimate the Curie temperature in these materials, though a comparison with $Ga_{1-x}Mn_xAs$ grown above the solubility limit shows a similar divergence and Tc not equivalent to that of the dilute alloy or secondary magnetic phase. A similar behavior for the magnetism is seen in the MOCVD-grown samples co-doped with silicon, where prior to co-doping, a large magnetic moment per atom can be seen. The magnetic moment decreases with increasing Si doping concentration and is nearly destroyed upon a target doping concentration greater than $10^{19}/cm^3$ Si.

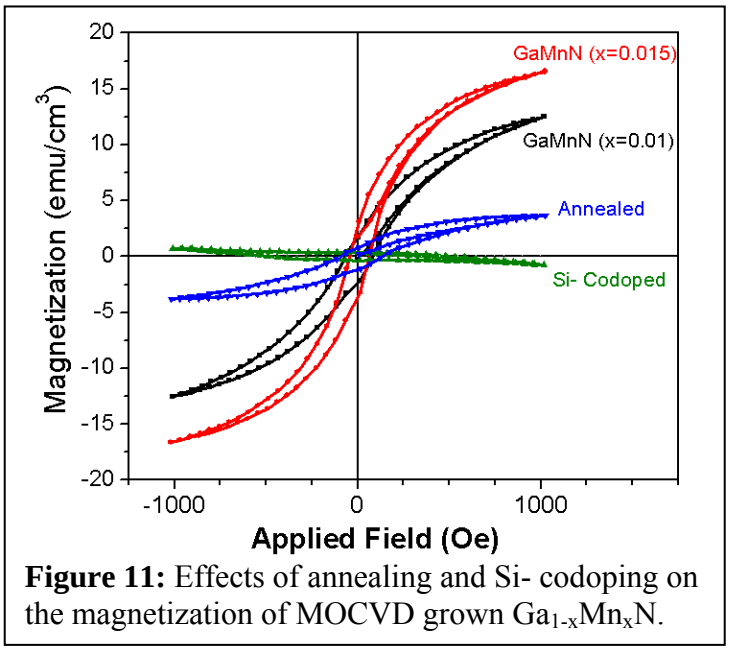

Figure 11: Effects of annealing and Si- codoping on the magnetization of MOCVD grown $Ga_{1-x}Mn_xN$.

The large decrease in the magnetization with co-doping and annealing suggests a common origin to the deterioration of the magnetic properties of $Ga_{1-x}Mn_xN$. This can be understood within the framework of filled and un-filled Mn impurity band states (i.e. double exchange mechanism), as this empirically seems to be the best model to describe the observed behavior if

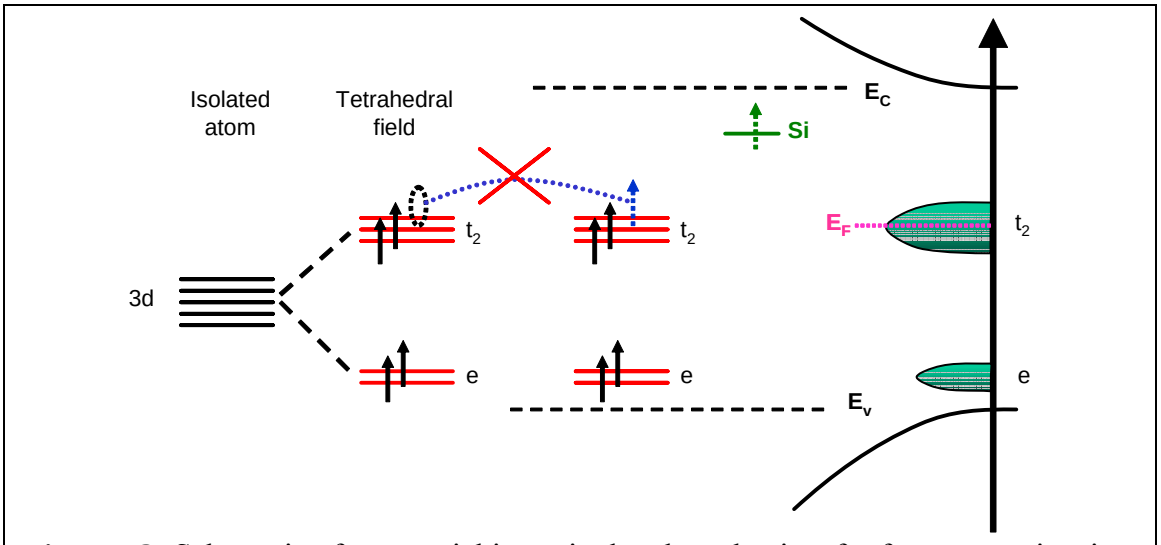

Figure 12: Schematic of a potential impurity band mechanism for ferromagnetism in $Ga_{1-x}Mn_xN$.

indeed it is due to the dilute alloy. In order to be able to support ferromagnetism, the Fermi level of the system must be in the spin split DOS Mn-impurity band, which is essentially midgap. The Fermi level must lie below the $Mn^{2+/3+}$ acceptor level so that the t_2 band is only partially filled and can support hopping and double exchange that stabilizes the ferromagnetism. Increasing the Fermi level by introducing donor states above this level results in trapping of donor electrons filling the t_2 band and a conversion from the Mn^{3+} (d^4) to the Mn^{2+} (d^5) configuration, thus eliminating the hopping pathway necessary for ferromagnetic ordering (Figure 12). These donor states may be introduced by either intentional co-doping, in the case of Si co-doping, or by the introduction of vacancies and other shallow donor defects during the annealing process. The results explained hereafter show a close correlation between the optical properties and electron paramagnetic spectrum with the valence state variation and magnetic properties in this system, as described next.

6. Optical properties of MOCVD-grown $Ga_{1-x}Mn_xN$

Optical studies have been used to investigate the origin of the room temperature (RT) ferromagnetism (FM) observed in $Ga_{1-x}Mn_xN$ epilayers, in particular to reveal the charge state of the incorporated Mn ions incorporated in GaN. To clarify whether isolated Mn ions (as observed for bulk $Ga_{1-x}Mn_xN$ and $Ga_{1-x}Mn_xAs$) or the formation of an Mn induced impurity energy band are the primary cause for the observed ferromagnetism, transmission and PL emission studies were performed. The transmission spectra of four samples are shown in Figure 13. Both, the Mn content and/or the donor concentration were varied during the MOCVD growth. The latter was predominantly achieved by Si co-doping during the growth. The optical analysis suggests that the incorporation of Mn into the GaN layers during growth leads to an absorption band (dip in transition spectra) around 1.5 eV. The incorporation of Mn into GaN layers during MOCVD growth leads to a broad absorption band, a spectrally diffuse line around 1.5 eV with a larger linewidth (full width at half of maximum – FWHM) [6]. The intensity and linewidth of this band scale with Mn concentration; the absorption depth (FWHM of the absorption band near 1.4eV) is 1.8% (120meV) for the 1% Mn sample, and 6.0% (180meV) for the 1.5% Mn sample. These transitions have also been observed in MBE-grown and implanted GaMnN epilayers. Mn^{3+} transitions from the E state to the partially filled T_2 levels of the ^5D state are assigned to the observed absorption band and the broadening of these states is due to the high Mn concentration This absorption peak is not observed in nominally undoped GaN grown on sapphire (not shown here) and $Ga_{1-x}Mn_xN$ layers co-doped with silicon

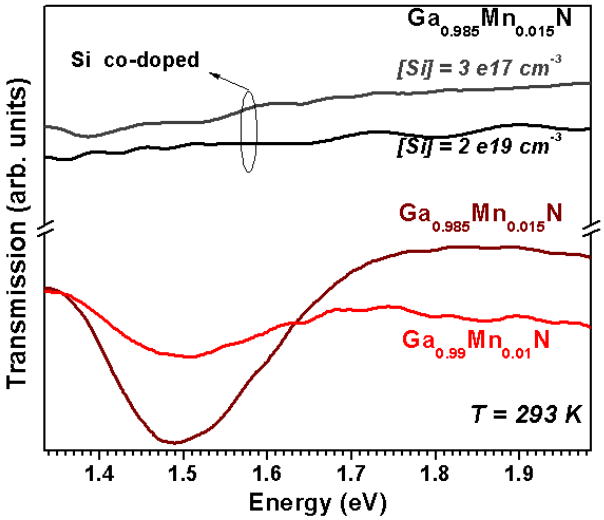

Figure 13: Optical transmission in $Ga_{1-x}Mn_xN$ samples with and without Si codoping. The absorption feature at 1.5 eV is indicative of Mn^{2+}

corresponding to a strong sensitivity to the position of the Fermi level. The absence of the absorption band around 1.5 eV in the $Ga_{1-x}Mn_xN$ layer co-doped with silicon indicates the sensitivity of the E to T_2 transitions to the position of the Fermi level. The Fermi level is shifted towards the conduction band because electrons are present at deep defects. No other absorption features were detected further in the infrared spectral range (down to 0.5 eV). This suggests that the location of the Fermi level in the investigated samples in the broad absorption band is around 1.8 eV above the top of the valence band, and even closer to the conduction band than for the Si co-doped sample. However, an unambiguous proof that this Mn-induced band causes magnetism for RT FM via double exchange interaction is still needed and will be addressed by spin-sensitive spectroscopic techniques.

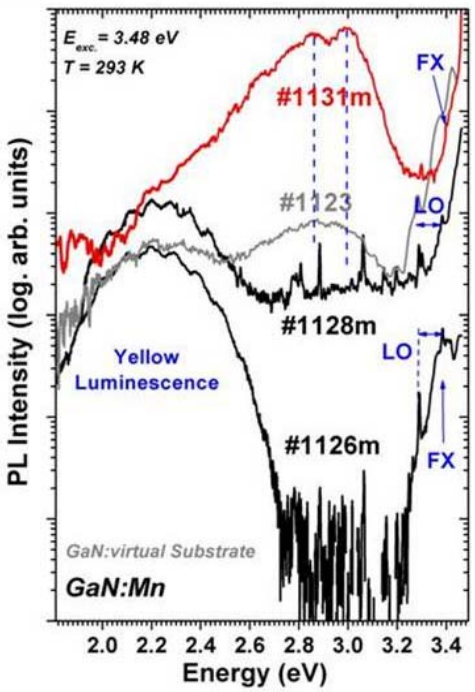

Figure 14: PL spectra from the MOCVD grown GaMnN layers. The distinctive peak around 3.0 eV appears with Mn introduction and may be due to Mn related defect complexes

Photoluminescence spectroscopy was used to investigate the defect levels present in the sample. Figure 14 shows PL spectra from 4 samples, 1123u, an undoped GaN layer, and three doped layers of increasing doping concentration and thickness (1126m, 1128m, and 1131m respectively). Despite the differences in the Mn concentration, similar behavior in both photoluminescence (PL) and transmission spectroscopy is observed for samples 1126m and 1128m, whereas different behavior of the PL was observed for the thicker sample 1131m. Here, the most prominent feature is the blue emission band around 3.0 eV. This band is similar to that observed in compensated Mg-doped GaN, but also reported in both ion-implanted and MBE-grown $Ga_{1-x}Mn_xN$ [7]. A transition from native defects (e.g. a nitrogen vacancy) and transition metal caused complexes is probably the origin of these emission bands. Reported peak energies for this emission band range from 2.90 eV [8] through 3.08 eV [7] at room temperature indicating the similarity to the respective band observed for compensated GaN:Mg, where different defect bands were resolved to contribute to the blue emission band [9]. The PL emission of the thin samples does not show this feature, as they are too thin relative to the underlying GaN layer. The dominating yellow band emission in those spectra is most likely due to defect centers in the GaN buffer layer. The transmission experiments revealed for sample 1131m an increase of detected light below 2.7 eV and a weak absorption signal around 1.75 eV. The latter is tentatively assigned to the emission of holes from the neutral Mn^{3+} acceptor state[10]. The increase in the transmission signal below 2.7 eV is in good agreement with the observed PL band around 3.0 eV and suggests resonant absorption by Mn-related states.[8] Assignment of these states is still somewhat controversial and the subject of continued investigations.

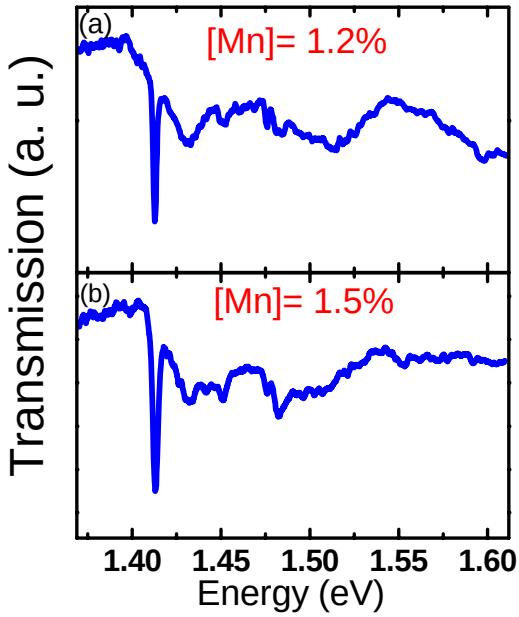

Figure 15: Transmission spectra of GaMnN at 4 K for Mn concentrations 1.2 % and 1.5 %. Note a scharp characteristic absorption at 1.41 eV of internal Mn-transition, with phonon replica on high-energy side. The zero phonon line broadens with increasing concentration of Mn.

Low temperature optical transmission has been used to confirm the presence of substitutional Mn and to monitor the change in the charge state of the transition metal ions. Figure 15 shows an internal transition from a Mn^{3+} ion through the transmission of luminescence back-excited from Cr^{3+} impurities in the sapphire substrate. A clear, distinct peak is observed in this scan near 1.41 eV, which is well-characterized as the zero phonon line of an internal forbidden d-d transition in Mn^{3+} (d^4) [10]. The observed absorption features are clearer than in any intentionally performed transmission measurements using a lamp-based excitation. Note the sharpness of the line at 1.7 K, which is inconsistent with a broad impurity-band like behavior. In addition to the sharp absorption zero phonon line, there are multiple phonon replicas at high energies. These, superimposed with Fabry-Perot oscillations from reflections of the film/substrate and film/air interfaces, are likely responsible for the observed band-like behavior at high temperature. There is some deviation in the transmission behavior at points over the wafer; this is consistent with both lateral fluctuation in the local Mn concentration due to 2-dimensional phase separation or simple variations in concentration across the wafer due to the gas flow injection patterns in the MOCVD reactor. Visual inspection of the $Ga_{1-x}Fe_xN$:Si films show a nonuniform yellowing color in some areas, which would be expected from Fe^{2+}.

Important to the overall electronic and magnetic behavior of the system is the local coordination and environment of the magnetic dopants. Electron paramagnetic resonance (EPR) was applied to study the incorporation and the electronic structure of the manganese ions. This technique uses microwave absorption in the presence of a magnetic field to observe transitions that are distinctive to the valence state of the impurity and its local atomic environment. The well resolved hyperfine structure allows an unambiguously identification of the impurity.

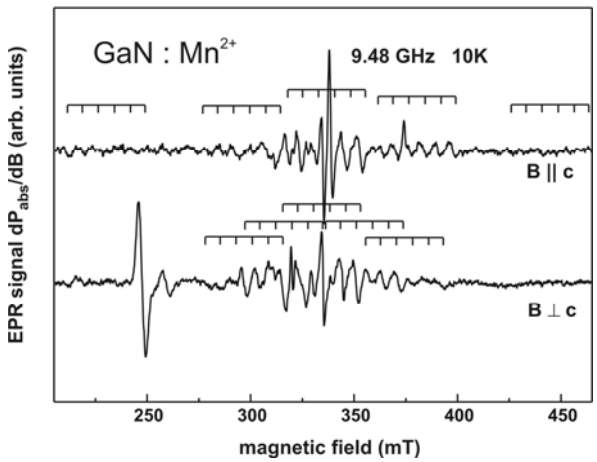

Figure 16: EPR signal as measured in an annealed MOCVD sample. The lines above the spectrum show the expected hyperfine line positions for Mn^{2+} in GaN, which correlate well to the observed lines

The observed resonance patterns shown in Figure 16 are well-described by the spin Hamiltonian for isolated $^{55}Mn^{2+}$ centers with electronic spin S=5/2 and nuclear spin I=5/2. The isotropic g factor and the isotropic hyperfine parameter A are identical with the values found for Mn-doped GaN-films grown by molecular beam epitaxy (MBE). The determined fine-structure parameter D of $240x10^{-4}$ cm^{-1} corresponds to values found for almost relaxed GaN-MBE films. It should be noted that this observation only occurs after annealing these samples, though the role, if any, of hydrogen passivation of the dopants is not yet understood. In addition, it is expected to find Mn^{3+} (= Mn^{2+} + hole) if the sample indeed exhibits hole-mediated ferromagnetism, which is not seen. The observation of this valence state is complicated by the presence of Cr^{3+} impurities in the sapphire substrate. The observed fine structure parameter is in agreement with Raman measurements. The measurements show only a small shift of the E_2 mode from the value for relaxed GaN. There is also no Raman shift nor peak broadening in the A_1(LO) mode, which indicates that significant strain is not introduced by the Mn introduction, and that the carrier concentration in the as measured samples is likely less than 10^{18} cm^{-3}. The EPR measurements provide the first direct evidence for Mn^{2+} incorporation in GaMnN, and prove that MOCVD can produce material of a similar or better quality with Mn-incorporation as that of the more well established DMS growth technique of MBE.

7. Raman investigations

The absence of Mn-induced strain was also confirmed by micro-Raman investigations. Raman spectra of GaMnN with different Mn and carrier concentrations are presented in Figure 17. Raman spectra of GaN epilayers grown on sapphire and on silicon are shown for comparison. Most prominent in all these spectra are the E_2 (high) and the A_1 (LO) Raman modes that were detected at 567 cm-1 and 734 cm-1, respectively. These values are in good agreement with those measured for relaxed GaN revealing that no additional strain was introduced even though a high concentration of Mn ions (~10^{20} cm-3) was incorporated in the GaN. A high carrier concentration (above 10^{18} cm-3) was ruled out since no broadening of the A_1 (LO) mode and no LPP modes were detected. According to the stronger strain in the case of the Si substrate, the Raman modes of this sample are shifted to lower energies compared with the epilayers on sapphire.

Micro-Raman spectroscopy was performed to determine the influence of the Mn incorporation on the vibrational properties of MOCVD-grown GaMnN. The spectra were recorded at room temperature in back scattering geometry. Raman spectra were recorded for GaN epilayers varying in Mn concentration from 0 to 1.5%, as shown in Figure 17. Mn doping during the MOCVD growth of GaN caused the appearance of modes in the Raman spectra not typically observed for the GaN

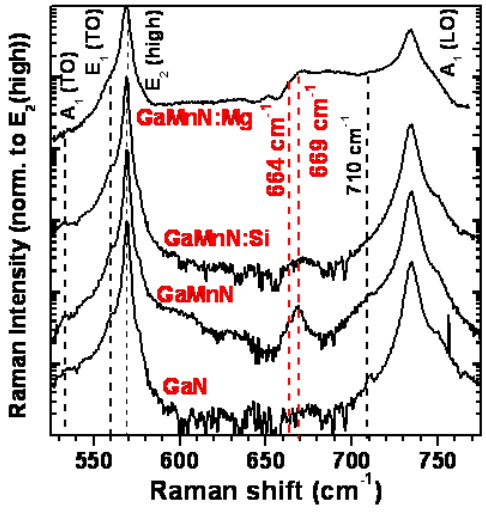

Figure 17: Raman spectra of $Ga_{0.985}Mn_{0.015}N$ with and without Mg and Si codoping. Note the sensitivity of the vacancy-induced local vibrational mode (LVM) at 669 cm^{-1} on co-doping

epilayers or the sapphire substrate. The appearance of a mode at ~ 669cm^{-1} and a shoulder at 664cm^{-1} were found strongly correlated to the Mn concentration. Its intensity, but not its linewidth increases with increasing Mn concentration. In this spectral range, a mode was found in GaN microcrystals at 670cm^{-1}, and it was assigned to a disorder-activated vibrational mode [11]. In another general study it has been reported that the mode is caused by vacancies in ion-implanted GaN epilayers [12]. In a more recent work based on MBE-grown $Ga_{1-x}Mn_xN$ this line was attributed to a local vibrational mode of the GaN host lattice caused by a vacancy. The data obtained from MOCVD-grown GaN and presented in this work appear to support the conclusions drawn by Harima [13].

An additional broad band around 300cm^{-1} that is disorder activated[11, 12, 14], did not show a systematic dependence on the Mn concentration but correlated more strongly with the crystalline quality determined by XRD, EPR and AFM [15]. In addition, the lower intensity of the 669cm^{-1} mode compared to that reported elsewhere[13] could be explained as a consequence of the MOCVD growth. Therefore, a GaN:Mn,Si sample was grown to study the role of vacancies. The Mn concentration was chosen as 1.5 % and the nominal Si concentration was ~10^{20} cm^{-3}. The incorporation of Si as a donor on Ga sites is known to reduce the amount of nitrogen vacancies in GaN [16]. Raman spectra of $Ga_{1-x}Mn_xN$ epilayers are shown in Figure 17. The intensity of the 669cm^{-1} mode increases with increasing Mn concentration, though the line width does not change. Also, it is obvious that upon Si co-doping the intensity of the 669cm^{-1} mode is strongly reduced. Moreover, the lack of plasmon-phonon coupled modes indicates that Mn was incorporated as an acceptor leading to the trapping of the electrons provided by the Si donors. However, further work is needed to confirm these results and assign these modes to their causes.

Local vibrational modes (LVMs) of Mn ions on Ga site based on the GaN E_2 (high) LO mode with respect to the difference in the reduced masses might be expected around 580cm^{-1}. However, no such mode was found in the GaMnN epilayers, and no phase separation was detected[17]. Unambiguous detection was prevented by the dominance of the GaN E_2 (high) LO mode and a mode near 576cm^{-1} that was also seen in bare Sapphire substrate. Here, resonant Raman experiments may reduce the influence of the sapphire.

8. Device Work

GaN-based p-i-n structures with Mn integrated into the intrinsic region have been grown to further investigate the fundamental properties of $Ga_{1-x}Mn_xN$ layers within GaN-based structures $Ga_{1-x}Mn_xN$ layers at approximately 1% Mn doping level were grown on n-doped GaN layers and subsequently capped with approximately 200 nm p-type layers. The Mn thickness was varied between 50nm and 200nm in order to investigate the thickness of the region on the behavior. The devices were then fabricated into diode structures using standard GaN LED lithographic techniques. I-V characteristics of the device structures clearly show rectifying behavior in the Mn p-i-n structures as shown via the light and dark curves in the inset Figure 18. With increasing Mn thickness, the turn-on voltage and resistance of the devices increases, as would be expected from the highly resistive nature of the centers. Figure 18 shows the electroluminescence (EL) behavior of a sample device. The EL spectra is dominated by two peaks – one at 3.4 eV which is due to the bandedge recombination, and another of approximately equal in magnitude at around 2.1 eV due to Mn-induced defected related emission. The intensity of the near-bandedge emission is several orders of magnitude lower than that of a GaN p-i-n

LED structure, and visibly, the Mn-containing emitters are more of a yellow-orange vice blue in color. With increasing thickness of the Mn, the area of light emission decreases, consistent with a higher spreading resistance of the device with the thicker Mn layer.

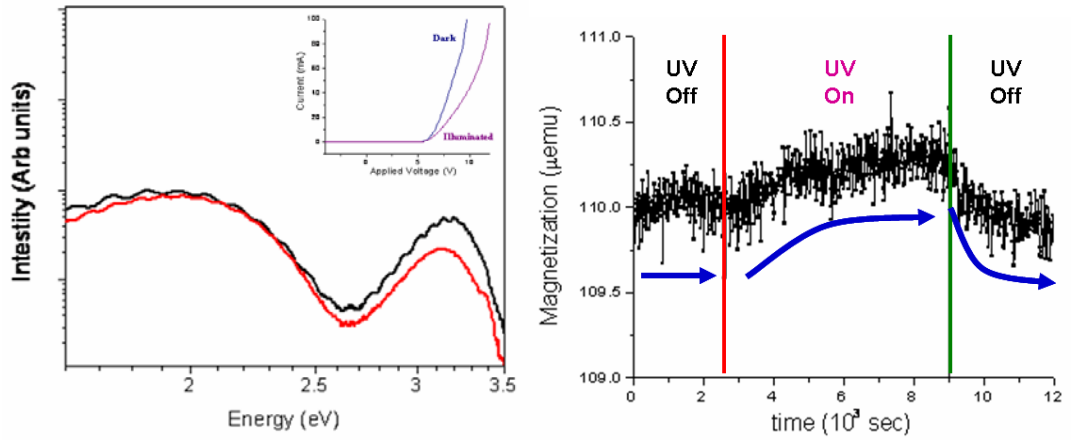

Figure 18: (a) Electroluminescence spectra of two p-i-n diodes with $Ga_{1-x}Mn_xN$ of varying thickness in the active region. The inset shows the light and dark I-V characterisic. (b) Measured VSM magnetization for 200 nm thick $Ga_{1-x}Mn_xN$ (x=0.015) layer with and without illumination from the unfiltered radiation of a UV lamp.

Another feature of $Ga_{1-x}Mn_xAs$ which has not been observed to date in $Ga_{1-x}Mn_xN$ is that of optically induced magnetization effects. By controlling the polarization of light near the band edge in $Ga_{1-x}Mn_xA$, carriers can be excited in sufficient quantities to result in an observed FM signal. Because of the deeper nature of the d-state related impurity band in $Ga_{1-x}Mn_xN$, optically induced magnetization will take on a different character. In order to study effects of a population of the band, VSM measurements were taken before and during excitation with the unfiltered, unpolarized light of an ultraviolet lamp, as shown in Figure 18. After illumination under the UV light, a rise in the measured magnetization can be seen. The effect is slight, less the 0.5% of the total magnetic signal as would be expected from the relative intensity of the source relative to the population of the traps, but above the inherent noise of the measurement and reversible with the illumination is removed. Investigations are underway to explore the spectral, radiant intensity, and polarization dependence of this phenomenon and to eliminate the possibility of any contribution from charging, heating, or other potential measurement-dependent effects.

9. Comparison of Mn and Fe in MOCVD-grown samples

Alternately, in order to circumvent the challenges with producing identical, near perfect material by a number of different techniques, another route towards understanding the various theories in place is to explore the role of various transition metals within the lattice. This is particularly important in the transition metal doped wide bandgap materials, as unusual behavior has been observed and predicted from transition metals which do not normally lead to magnetic behavior, such as Cu [18].

Moreover, the investigation of various transition metals enables the concurrent variation of a number of other parameters of interest in the various materials systems. In particular, the location of the acceptor level in III-V semiconductors is an important parameter, as it influences the

interaction of the magnetic center and band carriers (electrons or holes) in the carrier mediated model or polaronic radii and percolation threshold in a bound magnetic polaron model. The degenerate doping levels needed in these materials also can induce the formation of impurity bands and act as a pinning level for the Fermi energy. The location of this pinning level will also influence the materials properties and growth behavior, in particular the formation and nature of defects in GaN is sensitive to the position of the Fermi level within the bandgap [16]; the location of the pinned Fermi level may drive the system towards either V_n or Ga_i conditions. The use of various transition metals also allows for an exploration of the relationship of the observed ferromagnetism on filling of an impurity band. In Figure 19, the relative electronic configuration of Cr, Mn, and Fe in the high spin configuration within a tetrahedral crystal field environment are shown.

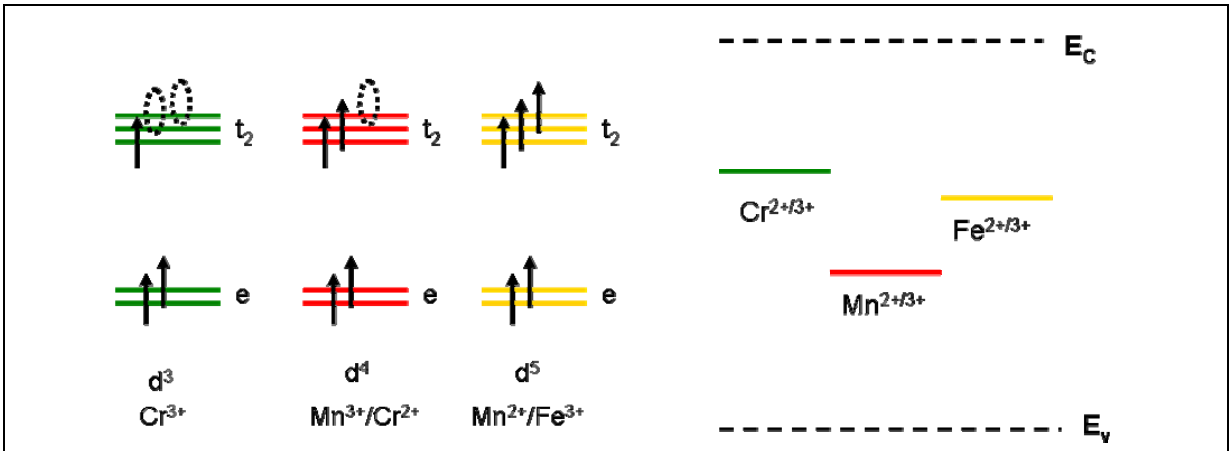

Figure 19: Schematic of the interior transition metal configurations and predicted positions within the bandgap of the $TM^{2+/3+}$ charge transfer level.

As the electronic configuration progresses from d^3 to d^5, in addition to the unpaired magnetization going from $3\mu_B$ to $5\ \mu_B$, the proposed impurity band levels go from one-third to completely filled, which should have a strong impact on the magnetic behavior in this model is valid. In addition, the relative position of the $TM^{2+/3+}$ acceptor level within the bandgap is also shown; the Mn level resides lower than either the Cr or Fe levels due to the a large correlation energy for Mn^{2+} in the d^5 configuration, which drives the acceptor level towards the valence band [19, 20]. At these relative energy levels, the formation of nitrogen vacancies is energetically more favorable [16], which could have a large effect on the nanoscale atomic ordering. In addition, some theoretical predictions have examined the role of various transition meals on the magnetic ordering within the system [6]. Comparing the observed properties with those predicted by first principles calculations can also provide some insight into the effectiveness in correlating the model with observed behavior. The magnetization is solely due to incommensurate impurities in a heterogeneous system, then the relative difference in these precipitate with transition metal doping should point to the physical nature of these precipitates. For example, Mn_4N is ferrimagnetic with a Tc of 743 K; while Fe_3N has a Tc of 535 K.

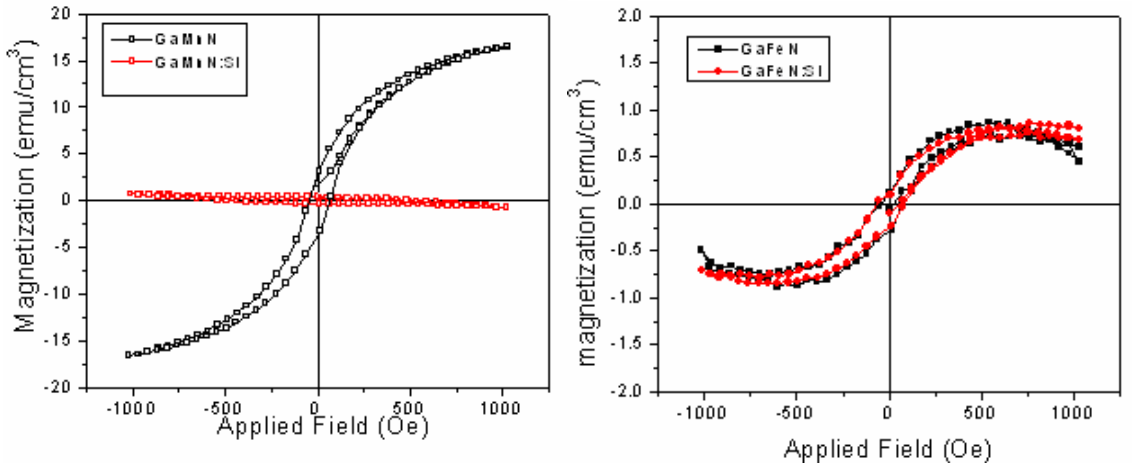

Figure 20: Magnetization as measured by SQUID of (a) $Ga_{1-x}Mn_xN$ (x=0.01) and (b) $Ga_{1-x}Fe_xN$ (x=0.003) taken at room temperature. A magnetic hysteresis is observed in both films, though the strength of the magnetization in considerably stronger in the Mn-containing films relative to the Fe containing films. Moreover, there is a strong dependence on the strength of the observed magnetization in the Mn-doped films with Si codoping at levels greater than 10^{19} cm^{-3}, which is not observed in the similarly doped Fe films.

The magnetization behavior of the films was determined by temperature-dependent SQUID magnetometry on Fe- and Mn-doped samples at temperature ranging 5 K to 300 K. Figure 20 shows the magnetic hysteresis curves of a lightly alloyed Mn (1%) and Fe (0.3%) GaN as measured by molar flow ratio samples. All graphs have been normalized by the volume of the sample as estimated from in-situ monitoring of the sample growth rate, time, and area. In both samples there is a clear evidence of magnetic hysteresis and room temperature ferromagnetism of undetermined origin in these samples. Note that ferromagnetism was achieved despite both the Mn and free hole concentration as measured by Hall effect and Raman spectroscopic measurements being far lower than that required by the free carrier mediated mean field theory [21]. Also shown in Figure 20 is the effect of high levels of Si co-doping on the magnetic properties as measured materials properties. With additional Si incorporation, there is no significant change in the carrier concentration as measured by Hall effect measurements in any of the samples, likely due to parallel conduction through the template layer. Secondary ion mass spectrometry has verified that the level of Mn-incorporation for a given flow rate of the precursor gas is not altered by Si. In contrast to the structural properties, there is a large difference, however in the observed strength of the magnetization in these samples. The temperature dependence of the zero-field cooled and field cooled magnetization versus temperature curves (not shown) indicates that the T_C of the magnetic phase is well above room temperature and higher in the Mn doped samples than the Fe doped samples. A comparison of the zero field cooled and field cooled magnetization plots at 100 Oe showed no evidence for superparamagnetic clusters as the source of the observed hysteresis. Still, the observed strong magnetization could be a result of the improved crystalline quality of the $Ga_{1-x}Mn_xN$ films relative to the $Ga_{1-x}Fe_xN$ films, the interaction of the transition metal with the increased number of structural vacancies, or an enhanced clustering enabled by easier diffusion through the vacancy-rich Mn-alloyed materials.

10. Clustering Evidence

Figure 20 shows the results of the magnetization scans taken at room temperature via DC SQUID magnetometry. Room temperature magnetic hysteresis is observed in both the Mn and Fe doped samples, even at relatively dilute alloying concentrations (0.3%). Such a doping level is far less than the percolation threshold needed in either a double exchange or impurity-band mediated model for ferromagnetism in these systems [22]. In Figure 2, the measured magnetization from the SQUID has been normalized to the film volume based on the growth rate of the film as measured by in situ reflectivity. Hysteresis curves for both the Fe and Mn alloyed samples show a distinct parallelogram-like shape instead of the more square shaped hysteresis loop shapes typically observed in $Ga_{1-x}Mn_xAs$; this has been attributed to non-uniform cluster distributions in these samples. With increasing silicon doping, the strength of the measured magnetization decreases considerably in the Mn doped samples; there is roughly no change in the magnetization of the Fe doped samples and a hysteretic magnetic signal persists in all of the measured curves. Secondary ion mass spectrometry (SIMS) has confirmed that there is no systematic variation in the overall incorporation of Mn, save for some local lateral fluctuations across the wafer described in more detail below.

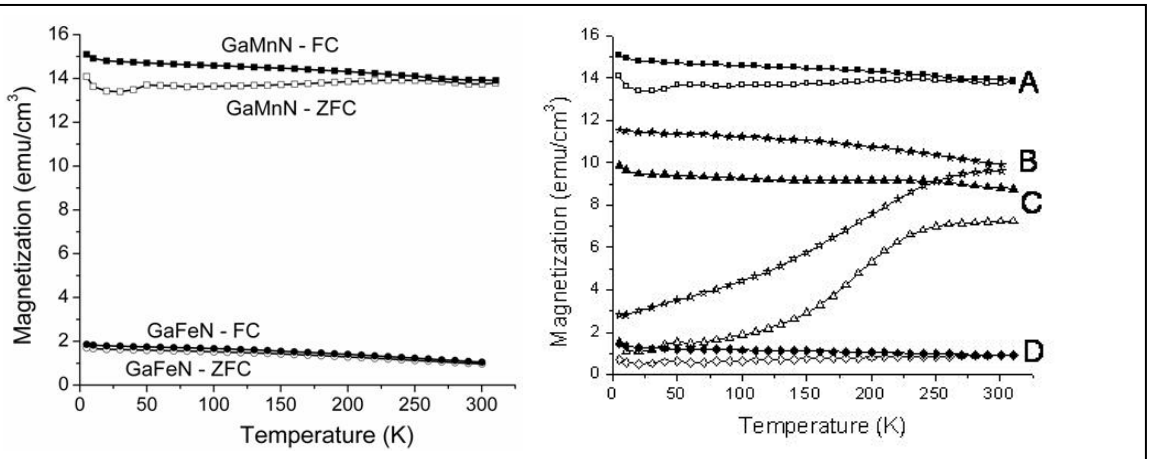

Figure 21: (a) FC (filled symbols) and ZFC (unfilled symbols) magnetization versus temperature curves for $Ga_{1-x}Mn_xN$ (x=0.015, circles) and $Ga_{1-x}Fe_xN$ (x=0.003, squares) (left). (b) FC (filled symbols) and ZFC (unfilled symbols) magnetization versus temperature curves for $Ga_{1-x}Mn_xN$ (x=0.02) with increasing molar flow rates of silane where A = 0 (■); B = 34 (★); C = 250 (▲) ; D= 923 (◆) (right).

The zero field cooled and field cooled magnetization curves from as-grown films show no indication of a classical superparamagnetic cusp, Figure 21a. Three contributions exist to the overall measured magnetization – a Pauli paramagnetic contribution from the d^5 ions (Mn^{2+}/Fe^{3+}), a temperature independent Van Vleck paramagnetic contribution from the d^4/d^6 (Mn^{3+}/Fe^{2+}) ions, and an above room-temperature ferromagnetic contribution from an as-of-yet unidentified Mn-rich phase. Van Vleck paramagnetism has been previously reported from Cr^{2+} (d^4) and Fe^{2+} (d^6) ions in II-VI semiconductors [23]; more recently, it has been suggested to be the source of the temperature independent contribution in $Ga_{1-x}Fe_xN$ films [24]. The relative strengths of the temperature independent portions of the ZFC/FC curves is consistent with this

assignment, as the trivalent state of the Mn^{3+} ion has an even number of electrons, which is more conducive to Van Vleck paramagnetic behavior than the odd-numbered Fe^{3+} or Mn^{2+} (post-codoping) ions.

And interesting behavior is observed in the films with increasing Si codoping, Figure 21b. A pronounced superparamagnetic splitting reminiscent of a distributed sizes of magnetic nanoparticles can be observed in the ZFC/FC curves with increasing silane molar flow rate. This observation can be understood by looking at the role of silane on both the charge state of the manganese ions and the expected behavior of a group of magnetic nanoparticles of distributed size. The equation for the blocking temperature (T_b) of a magnetic cluster is given by equation:

$$T_b = \frac{KV}{k_b \ln\left(\tau_{\exp} / \tau_O\right)}$$

Equation 1

Where V is particle volume, K is the anisotropy constant, τ_{exp} is the measurement time, and τ_o is the lifetime due to the natural gyromagnetic frequency of the particles. The two parameters of particular importance in the T_b of the $Ga_{1-x}Mn_xN$ films are the magnetic anisotropy term and the volumetric term, as the blocking temperature scales linearly with each. The magnetic anisotropy term can be particularly high for the embedded MnN_x particles, due to the highly anisotropic nature of the polar wurtzite GaN films. Combined with the volume of the particles, this could lead to blocking temperatures well above room temperature, and an observed magnetic hysteresis in the films below the blocking temperature. Silicon has two effects on the growth of MOCVD-grown films which could affect these samples. One effect is the aforementioned reduction of the Mn valence state, which could result in an effective decrease in the order parameter and the inhibition of Mn-Mn interactions, resulting in spinodal decomposition. The second effect that silicon has is that of an antisurfactant, and it has been used as a nucleation center for the high temperature MOCVD growth of quantum dots [25]. Silicon on the GaN growth surface increases the local surface energy, and acts as a nucleation site for islands, which lowers the effective diffusion length of these atoms, and hence lowers the number of Mn-Mn interactions which are necessary for the formation of the Mn-rich phase. This results in an overall decrease in the volume of the nanoparticles, which in turn leads to a greater fraction of this assembly with lower T_b, and hence a more pronounced splitting in the ZFC/FC magnetization curves.

Though it might be expected that the Fe co-doped samples should also exhibit a similar decrease in the magnetization strength based on interaction of charged impurities, it should be noted that the absence of such a behavior in not surprising in light of the growth processes and relative concentrations of the Mn and Fe used. The growth rate for the Mn doped films in these studies was 0.4 μm/hr as monitored by in situ reflectivity during the growth process; for the Fe doped films, a higher growth rate of 0.9 μm/hr was employed. This allows for shorter diffusion distances and fewer Fe-Fe interactions. The lower precursor ratios, which lead to fewer transition metal ions on the surface, increase the surface diffusion path necessary to reach additional transition metal atoms on the surface, thus reducing the rate at which spinodal decomposition occurs. Morever, since the rates of bulk diffusion in GaN at typical MOCVD growth temperatures are considerably smaller than the surface diffusion lengths, 2-dimensional surface diffusion is the dominant effect that results in Mn-Mn interactions and Mn-rich phase formation.

As a result, the expected shape of the embedded nanoparticles is not spherical, but disc-like. As the major axis of these embedded nanoparticles would be perpendicular to the growth direction, their observation in cross sectional transmission electron microscopy would be almost impossible. The low alloying concentrations of Mn used in this study likely preclude the observation of the theoretically proposed columnar Konbu-phase [26]. More detailed reports on the structural properties of these films are given elsewhere [27], though the Fe films also have an increased surface roughness, which is consistent with lower overall surface diffusion lengths and more 3-dimensional growth. Conditions which promote longer diffusion lengths and smoother surfaces would also tend to promote Mn-Mn interactions and phase decomposition. The concurrent observation of the appearance of the superparamagnetic phase and the optical observation of the conversion of Mn^{3+} ions to Mn^{2+} is consistent with the recent predictions [28] of charged controlled phase separation in these semiconductor alloys.

11. GaN nanostructures

Nucleation studies of undoped GaN nanostructures were performed first. Significant developments have been made in the GaN nanostructure growth over the last year. Stranski-Krastanow (SK) like growth mode has been successfully demonstrated for GaN nanostructure on smooth AlN template layers. In depth studies were carried out to determine the GaN and GaTMN growth parameters. A series of systematic experiments were performed in which the temperature, V/III ratio, and the amount of material deposited were varied to investigate the dimensions and density of the GaN nanostructures grown on AlN epitaxial layers on sapphire substrates.

AlN growth is not easy to achieve due to high reactivity of Al. High growth temperature, high purity source materials, and oxygen-free ambient are required for high crystalline quality. A two-step growth technique in which a thin layer was grown first at a low temperature to prevent thermal damage of the substrate surface, and then the second layer was grown at a high temperature to obtain high quality AlN.

All of the AlN growths were performed on sapphire substrates. The first growth process in AlN growth is a prebaking step at 1100 ºC under H_2 ambient to clean the substrate surface and to recrystallize the substrate. After the pre-baking, the growth temperature is reduced to 550 ºC to grow a 20 nm thick AlN buffer layer. The primary purpose of this step is to relieve the lattice mismatch between the main AlN layer and the sapphire substrate and to provide seeds where AlN is grown. After LT AlN growth, the growth temperature increases above 1000 ºC for thermal activation of LT AlN film under ammonia background. This process provides recrystallization of LT AlN and nucleation

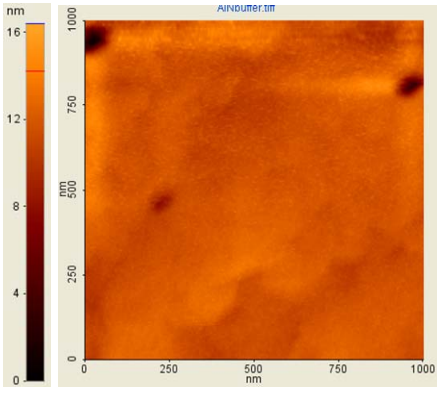

Figure 22: AFM image of AlN buffer layer.

The growth temperature for the high temperature AlN was optimized next. At lower growth temperatures, kinetic and thermodynamic energies are not sufficient to coalesce the AlN islands (i.e. grains) and crystallize. On the other hand, at excessively higher temperatures, these energies are so strong to leads to vertical growth, rather than lateral growth. The optimized growth temperature was determined to be at 1100 °C. Furthermore, the

optimal growth pressure was determined to be 50 Torr. At this pressure parasitic reactions are inhibited and lateral growth is promoted. The V/III ratio was also optimized with an optimal ammonia flow of 1.5 slm. Figure 22 shows the AFM image of the smooth AlN buffer with an RMS of less than 10 nm.

The optimization of the AlN buffer layer was followed by the growth of the GaN nanostructures. The strong impact of the growth temperature on the nanostructures' density and dimensions was confirmed by varying growth temperatures between 800°C and 1100°C.It was determined that 810°C is the favorable growth temperature as it resulted in comparatively smaller nanostructures with a high density. This relatively low temperature reduces both the kinetic energy of the atoms at the surface and the diffusion length, thereby supporting a 3D growth mode [29]. In this process the atoms are localized at the sites where they arrive at the surface instead of migrating to the edges of extended islands.

The V/III ratio is very important in nanostructure growth. Therefore, a wide range from 4.5-3500 was explored to determine the optimum conditions. Low V/III ratios favor 3D growth as it creates a metal rich condition that enhances the mobility of Ga atoms and enhances nucleation**.** Relatively low temperatures and extremely low V/III ratios are needed to form GaN nanostructures as shown in GaN QD growth on SiC [30]. Further, the deposition time was determined to control the size of the nanostructures and the amount of material deposited. Deposition time was kept as low as possible to enable a GaN deposition between two and 20 monolayers (MLs). The critical thickness for the transition from 2D to 3D growth is reported to fit in this range according to studies on SiC [30, 31]Silane was added to enhance nucleation in these experiments. AFM measurements resulted in nanostructures with lateral dimensions of 50 nm, height of 5 nm, and density of $3x10^9$ cm^{-2} for a V/III ratio of 20 and growth temperature of 810°C.

A further reduction in the nanostructure dimensions and an increase in their density were achieved using V/III ratios of less than 4.5. However, preliminary nucleation studies revealed that a thermal activation step after the deposition at ~810°C was necessary to promote the formation of nanostructures [32]. A temperature ramp was immediately applied in the reactor under a nitrogen atmosphere after GaN deposition for the activation step. A clear transition to 3D growth mode was observed for temperatures up to 970°C (Figure 23). This is because the temperature ramp increases the energy of the GaN atoms, which coalesce to from islands with smaller dimensions and larger height. AFM scans revealed nanostructures with a lateral dimension of 40 nm and height of approximately 4 nm with island densities of $1x10^{10}$ cm^{-2}. Temperature ramps above 1000°C result in an increase in lateral dimensions which can be attributed to the ripening of the islands. A similar technique for the formation of nanostructures by an *in-situ* activation step has been demonstrated for CdSe/ZnSe QDs [33]. The strong impact of the

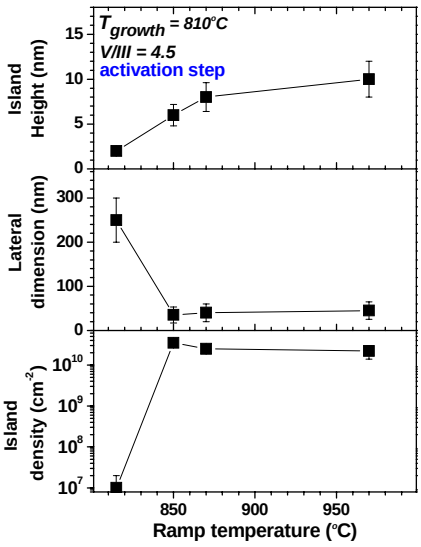

Figure 23: Density and dimensions of GaN/AlN nanostructures grown at 810°C and a V/III ratio of 4.5 as a function of the maximum temperature applied for the activation step.

activation temperature on the nanostructures' density and dimensions was further confirmed by performing *ex-situ* annealing in a RTA in a nitrogen atmosphere.

The physical properties of the nanostructures were studied in more detail by AFM and Raman spectroscopy. The nanostructure morphology and their density as obtained by AFM revealed an SK–like growth mode. The first critical thickness was observed at two MLs where the 2D growth (layer-by-layer growth) migrates into a 3D growth process. Thus, the thickness of the wetting layer is determined to be 2MLs. The density of the nanostructure increases beyond two MLs, while the size remains fairly constant. However, above eight MLs, the island density decreases and the lateral dimensions of the nanostructures increases, indicating the onset of a ripening process (Figure 24) [32, 34].

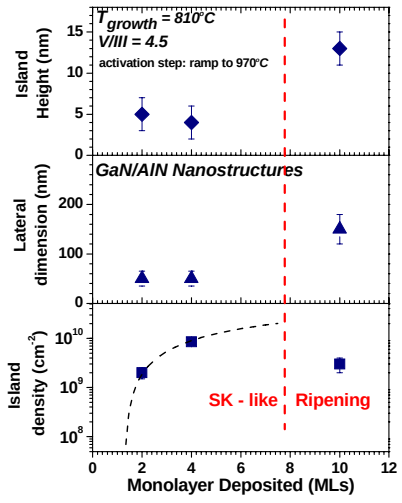

Figure 24: GaN / AlN nanostructure density and dimensions as a function of MLs deposited. Nanostructures begin to form at two MLs.

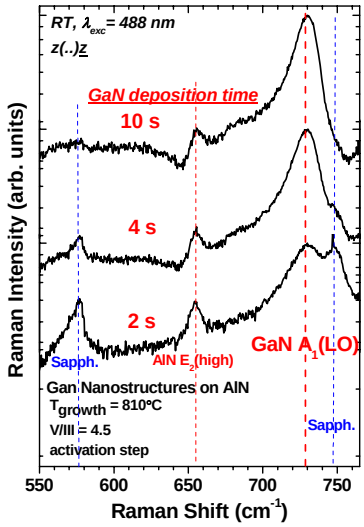

Figure 25: Raman spectra of GaN nanostructures for different GaN deposition times. The intensity of the GaN modes increases with the deposition time.

The Micro-Raman spectroscopy data obtained from these nanostructures grown with a V/III ratio of 4.5 and a temperature of 810°C followed by an activation step at 970°C is shown in Figure 25. The presence of the GaN A_1(LO) mode confirms the high crystalline quality of the nanostructures despite the extremely low V/III ratio and low growth temperature. Furthermore, the intensity of the GaN related Raman mode increases with deposition time (i.e., monolayer deposition), while the intensity of the observed AlN and sapphire related modes decreases.

PL measurements were conducted on GaN nanostructures which were capped with a thin AlN layer of

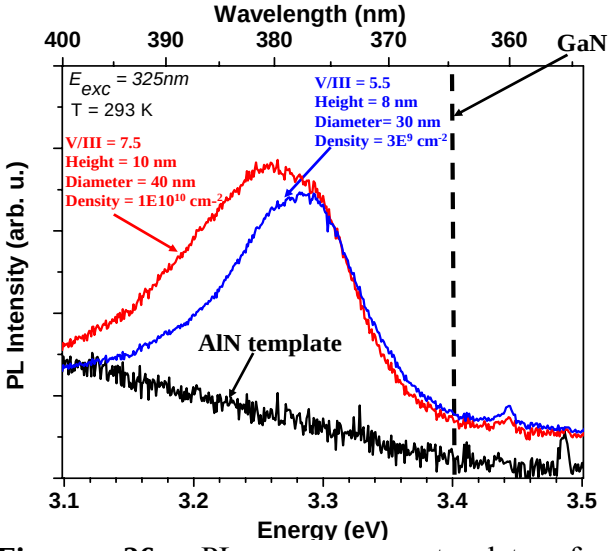

Figure 26: PL measurement data for GaN nanostructures. A blue shift in seen with a decrease in the nanostructure size.

approximately 50 nm. As seen in Figure 26, optically active nanostructures were obtained. The lattice mismatch between the AlN template and GaN islands, results in strained islands that increase the piezoelectric fields along the c-axis. The measured transition energies of the QDs is determined to be an interplay between the quantum size effect and the giant piezoelectric field along the c-axis [35].

It was observed that larger dots obtained at a higher V/III ratio resulted in a red shift. The shift to higher energies with a decrease in nanostructure size is attributed to the decrease in piezoelectric effect rather than quantum confinement. The intensity of the PL is dependent on the density of the nanostructures. A higher PL intensity is obtained with a higher density of nanostructures

Furthermore, a theoretical model has been created which showed that GaN nanostructures having a height smaller than 4.1nm have a larger bandgap energy than bulk GaN, while GaN nanostructures with height > 4.1nm has a smaller bandgap energy than the bulk GaN. Thus, confinement factor and piezoelectric field factor are offset each other at around a height of 4.1 nm where it is equal to the bandgap energy of bulk GaN (Figure 27a). Thus the height of the nanostructues is an important property to determine the excitonic properties. The results of this model were compared with the experimental results and were in good agreement as shown in Figure 27b.

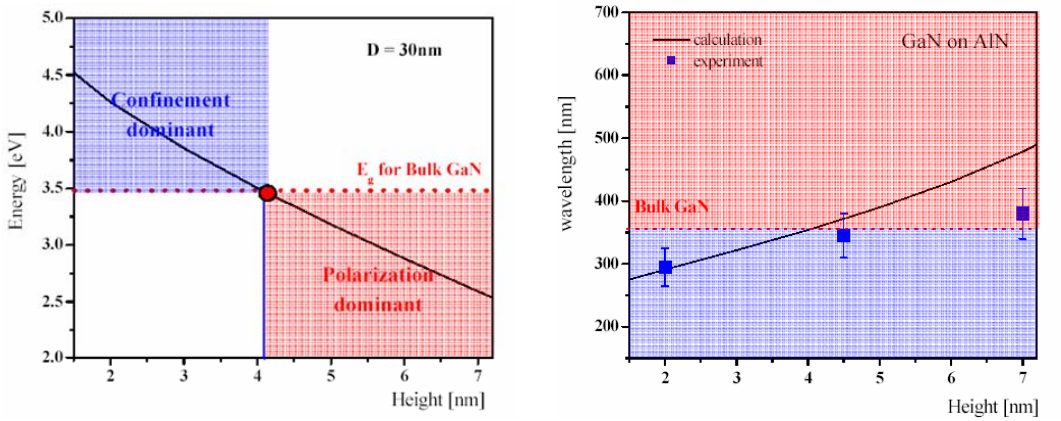

Figure 27: (a) Ground state exciton energies in GaN nanostructures as a function of height (left). (b) Comparison of experimental and calculated results of nanostructure optical emission as a function of height (right).

12. $Ga_{1-x}TM_xN$ nanostructures

To achieve multifunctional nanostructures initial nucleation studies on GaMnN grown on AlN epilayers were performed. Controlling the incorporation of transition metal ions in these nanostructures will enable control of their magnetic and optical properties. GaMnN nanostructures were grown by introducing Mn to GaN flows under the optimal conditions for the formation of nanostructures. The amount of Mn incorporated was calibrated by secondary ion mass spectroscopy measurements of bulk GaMnN layers [36]. Mn was varied from 0 to 2%, as beyond this composition phase segregation effects have been observed in bulk GaMnN layers [37]. Strain effects are not deemed to be significant at this level of composition as Mn and Ga are similar in size. The surface morphology was strongly affected by the presence of Mn atoms. The

AFM characterization (Figure 28) revealed the lateral dimension decreased to 30 nm and a height of 2 nm from the Mn deposition. Further, island density increased to $3.0x10^{10}$ cm^{-2}.

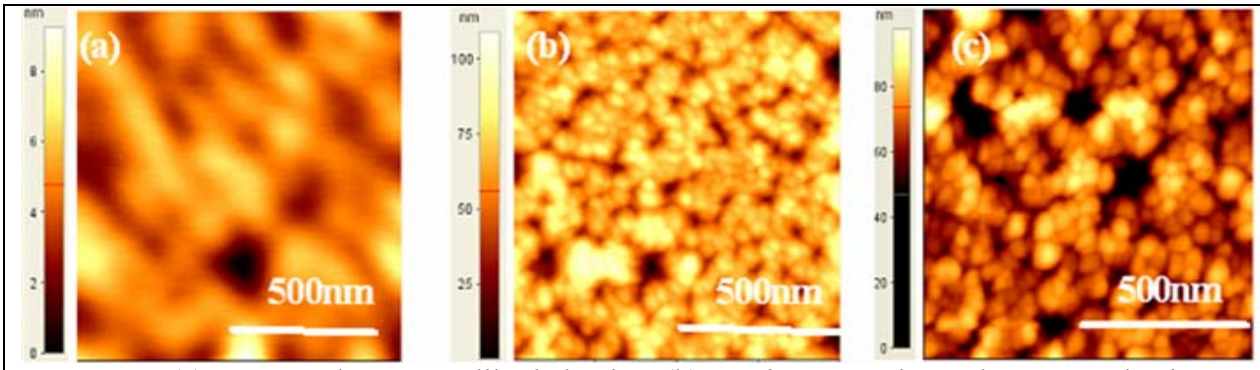

Figure 28: (a) 0% Mn shows 2-D like behavior. (b) Mn incorporation enhances nucleation and results in 3-D growth, resulting in increased island density and reduced lateral dimension. (c) An activation step above 880°C in GaMnN nanostructures leads to ripened islands.

No annealing step was necessary to provide small nanostructures of high density — unlike for the formation of GaN nanostructures as described above. In addition, the activation temperatures for the formation of nanostructures are significantly reduced, and above 880°C ripening processes lead to increased island dimensions and smaller island densities (Figure 28c). At this time, it may be speculated that the increase in the metal concentration (decrease in the V/III ratio), the role of Mn in enhancing nucleation, or both are responsible for the observed nucleation behavior of GaMnN nanostructures.

The $Ga_{1-x}Mn_xN$ nanostructures did not show signs of magnetization at RT. However, SQUID measurements on these nanostructures show a hysteresis behavior at 5K as shown in Figure 29. This provides evidence of ferromagnetism in $Ga_{1-x}Mn_xN$ nanostructures. RT ferromagnetism in $Ga_{1-x}Mn_xN$ nanostructures has not been achieved due to the degradation of the crystalline quality caused by the introduction of Mn. This result is a breakthrough in this area as till date magnetic signal has not yet been reported for $Ga_{1-x}Mn_xN$ nanostructures. Studies are underway to optimize the $Ga_{1-x}Mn_xN$ nanostructures growth process so as to achieve RT ferromagnetism.

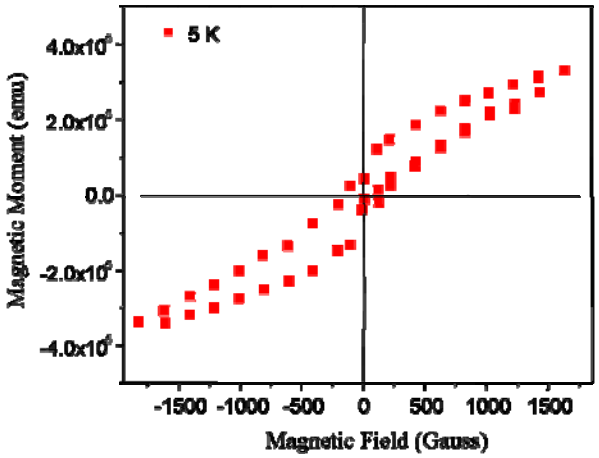

Figure 29: SQUID measurement of $Ga_{0.98}Mn_{0.02}N$ nanostructures taken at 5K.

Furthermore, the effect of Fe has been explored in these GaN nanostructures. For GaFeN nanostructure growth, up to 3 % Fe was introduced into GaN nanostructures under the optimal growth conditions accomplished for undoped GaN nanostructure growths. All samples for magnetization measurements had a 30-nm-thick AlN cap layer. The surface morphology was strongly affected by the existence of Fe atoms, as shown in Figure 30. The AFM characterization revealed a decrease in the lateral dimension to 30 nm and a height of 5 nm with 12 μmol/min flow of Fe precursor, and the island density increased to approximately $1x10^{10}$ cm^{-2}. The

presence of Fe leads to suppress adatoms migration due to altering surface free energy [38, 39] and enhances island formation. Therefore, it can be speculated that the increase in concentration of this transition metal is responsible for the observed nucleation behavior of GaFeN nanostructures.

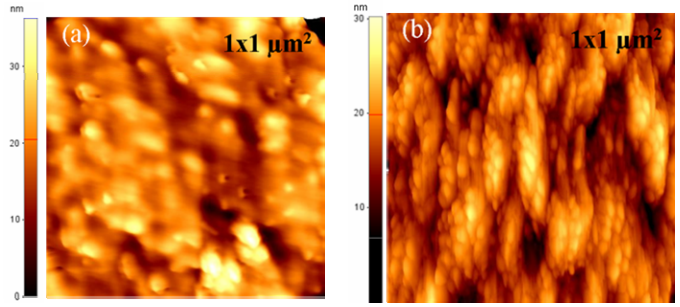

Figure 30: AFM image of $Ga_{1-x}Fe_xN$ with (a) 1% Fe incorporation and (b) 3% Fe incorporation.

Magnetization of GaFeN nanostructures has been revealed by VSM measurement at room temperature. As seen in Figure 31, the magnetization measurements show hysteresis loops of GaFeN nanostructures with different Fe doping levels at 293 K. The saturation magnetization increased from 5.3 µemu/cm^3 to 6.7 µemu/cm^3 and the coercivity increased from 7.7 Oe to 146.21 Oe as Fe was increased from 2 to 3 %. It is apparent that as the nanostructure size decreases and the density increases the saturation magnetization and coercivity increases. Thus, a larger amount of Fe incorporation reduces nanostructure size, and enhances ferromagnetism in the GaFeN nanostructures

The GaFeN nanostructures obtained in this study shows ferromagnetism at room temperature, which is just above the noise floor of the vibrating sample measurement technique in use. The curves shown in Figure 31 show the hysteresis curves after subtract a linear baseline which is a superposition of the sample holder and sapphire substrate and any paramagnetic contribution from isolated Fe centers in the sample. The exact nature of ferromagnetism in wide bandgap DMS is still controversial, but it may be possible to hypothesize based on the models in place at this time. The growth technique, assuming the Fe is contained within the nanostructure, promotes the concentration and nucleation at Fe containing sites. It also promotes the localization of carriers. Therefore, the growth of these nanostructures may promote more direct Fe-Fe interactions, as has been suggested in the cluster models for ferromagnetism in these systems. Moreover, the localization effects may assist the interaction of Fe with carriers trapped at defect sites in the dots themselves. The GaFeN nanostructure system is usually grown under metal-rich growth condition, which can easily generate the metallic interstitials. However, if the ferromagnetism of GaFeN can be explained using carrier mediated interactions between the Fe magnetic centers [40, 41] then the confinement in these nanostructures where free carriers are easily localized should enhance. The high concentration of localized carriers enhances exchanges between theses carriers and also

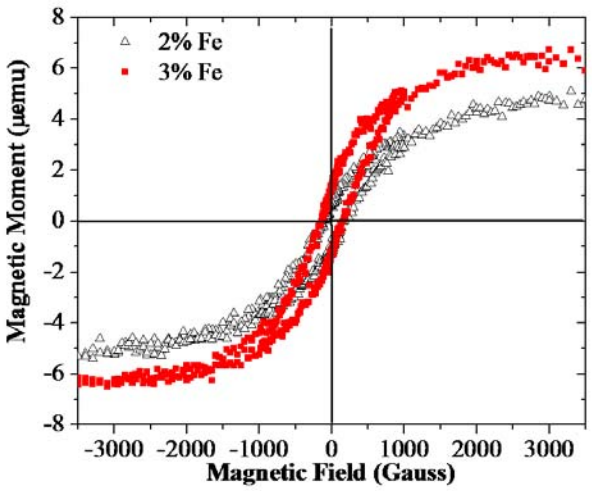

Figure 31: VSM measurement of $Ga_{1-x}Fe_xN$ nanostructures taken at 293K with x = 0.01 and 0.02.

localized spins of Fe impurity atoms, which implies stronger ferromagnetism It should be noted that in this case a higher Curie temperature (Tc > 293 K) has been observed in nanostructures than (Tc > 250 K) has been reported in the bulk system [24].

13. Conclusions

Overall, tremendous success and progress and has been obtained during the work on multifunctional III-Nitride QDs. This study explored in detail the effects of transition metal doping on GaN both at the bulk and QD level. Stranski-Krastanow like growth was demonstrated for the GaN nanostructures. Furthermore, it was demonstrated that the light emission can be red or blue shifted by controlling the size of the naostructures. The growth of GaMnN and GaFeN QDs were optimized and it was determined that transition metal enhance nucleation in Nitride QDs. This study is the first to demonstrate hysteresis curves for both GaMnN and GaFeN nanostructures.

Inaddition, at the bulk level, with the help of carrier codoping it was possible to justify the double exchange mechanism for the observed ferromagnetism. A more detailed systematic study using various transition metal elements as well as codoping elements suggests that the ferromagnetic behavior may not be an intrinsic property, and that controlled surface diffusion effects through antisurfactant codoping may lead to new functionalities within this materials system outside the traditional spintronic realm. In addition, this work combined materials science and electrical engineering in order to produce and analyze light emitting $Ga_{1-x}Mn_xN$ structures. The highly resistive nature of the Mn will complicate considerably the development of these devices. Lastly, this work has resulted in the training and intellectual development of two motivated engineering graduate students, and seeded numerous collaborations which should prove fruitful for future scientific endeavors.

Publications:

Book Chapter

[1] M. H. Kane, S. Gupta, H. Kang, and I. T. Ferguson, “Prospects for transition metal and rare earth doped nitrides for spintronics ”, In J. Miguel-Sánchez (Eds.), *Advances in the growth and properties of nitrides and diluted nitrides*, in progress.

Papers

[1] M. H. Kane, S. Gupta, W. E. Fenwick, N. Li, E. H. Park, M. Strassburg, and I. T. Ferguson, “Comparative study of Mn and Fe incorporation into GaN by metalorganic chemical vapor deposition”, Physica Status Solidi (A) Applied Research, vol. 204, pp. 61-71, 2007.

[2] S. Gupta, H. Kang, M. H. Kane, E. H. Park, and I. T. Ferguson, “Structural and magnetic characterization of MOCVD grown GaMnN and GaFeN nanostructures”, Mat. Res. Soc. Symp. Proc., Accepted for publication,2007.

[3] M. H. Kane, W. E. Fenwick, S. Gupta, N. Li, C. J. Summers and I.T. Ferguson," Comparison of the incorporation of various transition metals into GaN by MOCVD", Mat. Res. Soc. Symp. Proc., accepted for publication, 2007.

[4] M. H. Kane, S. Gupta, H. Kang, W. E. Fenwick, E. H. Park, E. Malguth, A. Hoffmann, M. H. Han, Z. J. Zhang, and I. T. Ferguson, "Evidence for silicon-induced inhibition of magnetic phase segregation in Ga1-xTM_xN (TM = Fe, Mn) films grown by MOCVD", Applied Physics letters, accepted for publication, 2007.

[5] M. H. Kane, M. Strassburg, W. E. Fenwick, A. Asghar, J. Senawiratne, D. Azamat, Z. Hu, E. Malguth, S. Graham, U. Perera, W. Gehlhoff, A. Hoffman, N. Dietz, C. J. Summers, and I.T. Ferguson, "Optical studies of MOCVD-grown GaN-based ferromagnetic semiconductor epilayers and devices", Physica Status Solidi (C), No. 6, pp. 2237-40, 2006.

[6] W. E. Fenwick, A. Asghar, S. Gupta, H. Kang, M. Strassburg, N. Dietz, S. Graham, M. H. Kane, and I. T.Ferguson, "Manganese-induced long-range lattice disorder and vacancy formation in metal-organic chemical vapor deposition grown and ion-implanted $Ga_{1-x}Mn_xN$", Journal of Vacuum Science and Technology A: Vacuum, Surfaces and Films, vol. 24, pp.1640-1643, 2006.

[7] M. H. Kane, M. Strassburg, A. Asghar, W. E. Fenwick, J. Senawiratne, Q. Song, C. J. Summers, Z. J. Zhang, N. Dietz, and I. T. Ferguson, "Alloying, co-doping, and annealing effects on the magnetic and optical properties of MOCVD-grown $Ga_{1-x}Mn_xN$", Materials Science and Engineering B, vol. 126, pp.230-235, 2006.

[8] S. Gupta, H. Kang, M. H. Kane, W.E. Fenwick, N. Li, M. Strassburg, A. Asghar, N. Dietz, and I. T. Ferguson, "MOCVD growth of GaN and GaMnN multifunctional nanostructures", Mat. Res. Soc. Symp Proc., vol. 901E, pp. 0901-Ra13-04.1- 0901-Ra13-04.6, 2006.

[9] M. H. Kane, M. Strassburg, W. E. Fenwick, A. Asghar, A. M. Payne, S. Gupta, Q. Song, Z. J. Zhang, N. Dietz, C. J. Summers, and I. T. Ferguson, "Correlation of the structural and ferromagnetic properties of $Ga_{1-x}Mn_xN$ grown by metalorganic chemical vapor deposition", Journal of Crystal Growth, vol. 287, pp. 591-595, 2006.

[10] M. H. Kane, M. Strassburg, A. Asghar, N. Li, W. E. Fenwick, and I. T. Ferguson, "Review of Recent Efforts on the Growth and Characterization of Nitride-based Diluted Magnetic Semiconductors", Proceedings of SPIE, vol. 6121, pp. 173-187, 2006.

[11] M. H. Kane, M. Strassburg, W. E. Fenwick, A. Asghar, and I. T. Ferguson, "The Growth and Characterization of Ferromagnetic Wide Bandgap Materials for Spintronic Applications", International Journal of High Speed Electronics,vol.16, No 2, pp. 515 543, 2006.

[12] M. Strassburg, M. H. Kane, A. Asghar, Q. Song, Z. J. Zhang, J. Senawiratne, M. Alevli, N. Dietz, C. J. Summers, and I.T. Ferguson, "The Fermi level dependence of the optical and magnetic properties of $Ga_{1-x}Mn_xN$ grown by metal-organic chemical vapour deposition", Journal of Physics Condensed Matter, vol. 18, pp. 2615-2622, 2006.

[13] Z.G. Hu, M. Strassburg, N.Dietz, A.G.U. Perera, M.H. Kane, A. Asghar, and I.T. Ferguson, "Effect of Mn composition on E1(TO) phonon mode in hexagonal $Ga_{1-x}Mn_xN$ epitaxial films on c-plane sapphire substrates", Applied Physics Letters, vol. 88, pp. 061914, 2006.

[14] S. Gupta, H. Kang, M. Strassburg, A. Asghar, M. H. Kane, W. E. Fenwick, N. Dietz, and I. T. Ferguson, "A nucleation study of group III-Nitride multifunctional nanostructures", Journal of Crystal Growth, vol. 287, pp. 596-600, 2006.

[15] M. H. Kane, A. Asghar, A. M. Payne, C. R. Vestal, M. Strassburg, J. Senawiratne, Z. J. Zhang, N. Dietz, C. R. Summers, and I. T. Ferguson, "Magnetic and optical properties of GaMnN grown by Metalorganic Chemical Vapor Deposition", Semiconductor Science and Technology, vol. 20, pp. L5-L9, 2005. ***(Note: Paper also selected for recognition in Institute of Physics Select issue as research which shows "substantial advances or significant breakthroughs, a high degree of novelty, and a significant impact on future research").***

[16] M. H. Kane, A. Asghar, A. M. Payne, C. R. Vestal, Z. J. Zhang, M. Strassburg, J. Senawirante, N. Dietz, C. J. Summers, and I. T. Ferguson, "Comparison of GaMnN epilayers prepared by ion implantation and metalorganic chemical vapor deposition", Physica Status Solidi (C), vol. 2, No. 7, pp. 2441–2445, 2005.

[17] M. H. Kane, A. Asghar, M. Strassburg, Q. Song, A. M. Payne, C. J. Summers, Z. J. Zhang, N. Dietz, and I. T. Ferguson, "Impact of Manganese incorporation on the structural and magnetic properties of MOCVD-grown $Ga_{1-x}Mn_xN$ ", Materials Research Society Proceedings, vol. 831, pp. E9.4.1-E9.4.6, 2005.

[18] M. Strassburg, J. Senawirante, C. Hums, N. Dietz, M. H. Kane, A. Asghar, A. M. Payne, I. T. Ferguson, C. J. Summers, U.Haboeck, A. Hoffman, D. Azamat, and W. Gelhoff, "Optical and Structural Investigations on Mn-Ion States in MOCVD-grown $Ga_{1-x}Mn_xN$ ", Materials Research Society Proceedings, vol. 831, pp. E9.5.1-E9.5.6, 2005.

[19] M. H. Kane, M. Strassburg, A. Asghar, Q. Song, S. Gupta, J. Senawiratne, C. Hums, U. Haboeck, A. Hoffmann, D.Azamat, W. Gehlhoff, N. Dietz, Z. J. Zhang, C. J. Summers, and I. T. Ferguson, "Multifunctional III-nitride dilute magnetic semiconductor epilayers and nanostructures as a future platform for spintronic devices ", SPIE Proc., vol. 5732, pp. 389-400, 2005.

[20] S. Gupta, H. Kang, M. Strassburg, A. Asghar, J. Senawiratne, N. Dietz, and I. T. Ferguson, "A nucleation study of GaN multifunctional nanostructures", Mat. Res. Soc. Symp. Proc., vol. 831, pp. 759-764, 2005.

Presentations:

[1] M. H. Kane, S. Gupta, W. E. Fenwick, E. H. Park, M. H. Han, Z. J. Zhang, E. Malguth, A. Hoffmann and I.T. Ferguson,"Surface Diffusion Effects on the Magnetic Properties on MOCVD-grown GaMnN and GaFeN", presented at Mat. Res. Soc. Symp., Spring meeting, San Francisco, CA, April, 2007.

[2] M. H. Kane, S. Gupta, W. E. Fenwick, N. Li, E.H. Park. M. Strassburg, and I. T. Ferguson,"Comparative study of Mn and Fe incorporation into GaN by metalorganic chemical vapor deposition", presented at European Materials Research Society Conference, Warsaw, Poland, September 2006.

[3] **Invited:** I. T. Ferguson, "Spin dynamics of Dilute Magnetic Quantum Dots", presented at the International Conference on Superlattices, Nanostructures and Nanodevices, Istanbul, Turkey, August 2006.

[4] M. H. Kane, "Transition metal doped GaN and ZnO for Spintronic Applications", presented at Technical University Berlin,Institute of Solid State Physics seminar, February 2006.

[5] M. H. Kane, "Wide bandgap ferromagnetic semiconductors: Novel materials development for next-generation electronics", presented at the University of California - Davis, Department of Chemical Engineering and Materials Science seminar, January 2006.

[6] **Invited:** M. H. Kane, W. E. Fenwick, M. Strassburg, A. Asghar, N. Li, and I. T. Ferguson,"Exploration of the growth and suitability of nitride-base semiconductors for ferromagnetic semiconductor spintronics", presented at Photonics West, San Jose, CA, January, 2006.

[7] M. H. Kane, "Chemistry and Physics of $Ga_{1-x}Mn_xN$, a new magnetic semiconductor material", presented at the Virginia Military Institute, Department of Physics and Chemistry seminar, December 2005.

[8] N. Li, W.E. Fenwick, M. H. Kane, M. Strassburg, A. Asghar, N. Dietz and I.T. Ferguson, "Magneto-Optical and Structural Studies on Mn Ion States in MOCVD-grown GaMnN", presented at Materials Research Society Fall Meeting, Boston, MA, November 2005.

[9] S. Gupta, H. Kang, M. Strassburg, A. Asghar, M. H. Kane, W. E. Fenwick, N.Dietz, and I.T.Ferguson, "MOCVD Growth of GaN and GaMnN Multifunctional Nanostructures", presented at Materials Research Society Fall Meeting, Boston, MA, November 2005.

[10] M. H. Kane, M. Strassburg, W. E. Fenwick, A. Asghar, and I. T. Ferguson, ”Growth of Nitride-based Ferromagnetic Semiconductors for Room Temperature Spintronic Applications”, presented at Institute of Physics Workshop on Spintronics and Nanomagnetism, London, England, September 2005.

[11] M. H. Kane, M. Strassburg, W. E. Fenwick, A. Asghar, J. Senawiratne, Q. Song, D. Azamat, M. Wagner, U. Haboeck, Z.Hu, Z. J. Zhang, U. Perera, W. Gehlhoff, A. Hoffmann, N. Dietz, C. J. Summers, and I. T. Ferguson, “MOCVD-growth of Nitride-based Ferromagnetic Semiconductors”, presented at the 6th International Conference on Nitride Semiconductors, Bremen, Germany, September 2005.

[12] M. H. Kane, M. Strassburg, A. Asghar, S. Gupta, H. Kang, N. Dietz, and I. T. Ferguson, “MOCVD-growth of GaN-based Ferromagnetic Semiconductors”, presented at the 12th US Biennial Workshop on Organometallic Vapor Phase Epitaxy, Big Sky, Montana, July 2005.

[13] S. Gupta, H. Kang, M. Strassburg, A. Asghar, N. Dietz, and I. T. Ferguson, “A Nucleation Study of Group III-Nitride Multifunctional Nanostructures”, presented at the 12th US Biennial Workshop on Organometallic Vapor Phase Epitaxy, Big Sky, Montana, July 2005.

[14] M. H. Kane, M. Strassburg, A. Asghar, and I. T. Ferguson, “Ferromagnetism in GaN-based Materials: Experiment versus Theory”, presented at the International Workshop on Wide Band Gap Ferromagnetic Semiconductors, Edinburgh, Scotland, May 2005.

[15] A. Hoffmann, E. Malguth, W. Gehlhoff, M. Strassburg, N. Dietz, M. H. Kane, and Ian T. Ferguson, “Transition metal ions in wide bandgap semiconductors - a challenge for spintronic applications”, presented at the International Workshop on Wide Band Gap Ferromagnetic Semiconductors, Edinburgh, Scotland, May 2005.

[16] M. H. Kane, A. Asghar, M. Strassburg, S. Gupta, W. E. Fenwick, Q. Song, U. Haboeck, A.Hoffmann, D. Azamat, W. Gehlhoff, C. J. Summers, Z. J. Zhang, N. Dietz, and I. T. Ferguson, "Growth of $Ga_{1-x}Mn_xN$ epilayers and nanostructures toward functional semiconductor spintronics", presented at Nanoscale Devices and Systems Integration Conference, Houston, TX, April 2005.

[17] M. Strassburg, M. H. Kane, A. Asghar, J. Senawirante, M. Alevli, C. Hums, N. Dietz, C. J.Summers, Ian T. Ferguson, U. Haboeck, A. Hoffmann, D. Azamat, and W. Gehlhoff, “MOCVD-grown $Ga_{1-x}Mn_xN$ Epilayers and Nanostructures”,presented at the Annual Spring meeting of the German Physics Society (DPG), Berlin, Germany, March 2005.

[18] C. Hums, M. Strassburg, M.H. Kane, A. Asghar, J. Senawiratne, M. Alevli, N. Dietz, C.J. Summers, I.T. Ferguson, and A. Hoffmann, “Fermi level dependence of optical and magnetic properties in MOCVD-grown GaMnN”, presented at the Annual Spring meeting of the German Physics Society (DPG), Berlin, Germany, March 2005.

[19] M. H. Kane, A. Asghar, M. Strassburg, J. Senawiratne, Z. J. Zhang, D. Azamat, U. Haboeck, A. Hoffmann, W. Gehlhoff, N. Dietz, C. J. Summers, and I. T. Ferguson, "Room temperature ferromagnetism in semiconductors: Data vs. Theory", presented at ARO Workshop on Room Temperature Ferromagnetism in Semiconductors, Gainesville, FL, March 2005.

[20] **Invited:** M. H. Kane, A. Asghar, A. M. Payne, C. R. Vestal, M. Strassburg, J. Senawiratne, Z. J.Zhang, N. Dietz, C. J. Summers, and I. T. Ferguson, "Wide-bandgap diluted magnetic semiconductors as a future platform for spintronic sensors", presented at Photonics West, San Jose, CA, January 2005.

[21] M. H. Kane, "Wide bandgap ferromagnetic semiconductors: Novel materials development for next-generation electronics", presented at ASM Atlanta Chapter meeting, Atlanta, GA, January 2005.

[22] M. H. Kane, A. Asghar, M. Strassburg, Q. Song, A. M. Payne, C. J. Summers, Z. J. Zhang, N. Dietz, and I. T. Ferguson, "Impact of Manganese incorporation on the structural and magnetic properties of MOCVD-grown $Ga_{1-x}Mn_xN$ ", presented at Materials Research Society Fall Meeting, Boston, MA, November 2004.

[23] M. H. Kane, "Development of Wide Bandgap Semiconductors for Spintronics", presented at Materials Research Society Fall Meeting, Boston, MA, November 2004 (*graduate student award presentation*).

[24] M. H. Kane, A. Asghar, A.M. Payne, C.R. Vestal, Q. Song, M. Strassburg, J. Senawiratne, Z.J. Zhang, N. Dietz, C. J. Summers, and I.T. Ferguson, "Wide-bandgap diluted magnetic semiconductors as a future platform for spintronic sensors", presented at Georgia Tech 5th Annual Conference on Nanoscience and Nanotechnology, Atlanta, GA, November 2004.

[25] M. H. Kane, V. Rengarajan, C. R. Vestal, K. Shalini, J. Nause, J. Z. Zhang, C. J. Summers, and I. T. Ferguson, "Another spin: can room temperature ferromagnetism be obtained in wide bandgap materials", presented at Conference on Quantum Electronics and Photonics, Glasgow, Scotland, September 2004.

[26] M. H. Kane, A. Asghar, C. R. Vestal, S. Gupta, D. Mehta, A. M. Payne, M. Strassburg, J. Senawiratne, N. Dietz, Z. J. Zhang, C. J. Summers, and I. T. Ferguson, "Comparison of GaMnN grown by ion implantation and metalorganic chemical vapor deposition", presented at International Workshop on Nitride Semiconductors, Pittsburgh, PA, July 2004.

[27] M. Strassburg, N. Dietz, D. Azamat, U. Haboeck, A. Hoffmann, W. Gehlhoff, M. H. Kane, A. Asghar, A. M. Payne, C. R.Vestal, Z. J. Zhang, C. J. Summers, and I. T. Ferguson,"Incorporation of Manganese on lattice site in MOCVD-grown $Ga_{1-x}Mn_xN$ ", presented at TMS Electronic Materials Conference, Notre Dame, IN, June 2004.

[28] M. H. Kane, A. Asghar, C. R. Vestal, Z. J. Zhang, C. J. Summers, T. Steiner, I. T. Ferguson, M. Strassburg, N. Dietz, D.Azamat, U. Haboeck, A. Hoffmann, and W. Gehlhoff, "MOCVD growth and characterization of Multifunctional III-Nitride Nanostructures", presented at 1st US-Korea Workshop on Nanoelectronics, Seoul, South Korea, May 2004.

[29] M. H. Kane, A. Asghar, C. R. Vestal, Z. J. Zhang, C. J. Summers, T. Steiner, I. T. Ferguson, M. Strassburg, N. Dietz, D. Azamat, U. Haboeck, A. Hoffmann, and W. Gehlhoff, "MOCVD growth and characterization of Multifunctional III-Nitride Nanostructures", presented at AFOSR Workshop on Nanoscale Issues in Nitride Semiconductors, Anchorage, AK, May 2004.

References

[1] I. T. Ferguson, "A New Spin for the Nitrides: Can Room Temperature Ferromagnetism be obtained in (Ga,Mn)N," Georgia Institute of Technology, Atlanta, GA, Annual Report ECS 0224266, 7/14/2003 2003.

[2] M. H. Kane, M. Strassburg, A. Asghar, W. E. Fenwick, J. Senawiratne, Q. Song, C. J. Summers, Z. J. Zhang, N. Dietz, and I. T. Ferguson, "Alloying, co-doping, and annealing effects on the magnetic and optical properties of MOCVD-grown Ga1-xMnxN," *Materials Science and Engineering: B,* vol. 126, pp. 230-235, 2006.

[3] D. Korakakis, K. F. Ludwig, and T. D. Moustakas, "Long Range order in AlxGa1-xN films grown by molecular beam epitaxy," *Applied Physics Letters,* vol. 71, pp. 72-74, 1997.

[4] M. L. Reed, N. A. El-Masry, H. H. Stadelmaier, M. K. Ritums, M. J. Reed, C. A. Parker, J. C. Roberts, and S. M. Bedair, "Room temperature ferromagnetic properties of (Ga, Mn)N," *Applied Physics Letters,* vol. 79, pp. 3473-3475, 19 Nov 01 2001.

[5] M. L. Reed, E. A. Berkman, M. J. Reed, F. E. Arkun, T. Chikyow, S. M. Bedair, J. M. Zavada, and N. A. El-Masry, "Magnetic properties of Mn-doped GaN, InGaN, And AlGaN," *Materials Research Society Proceedings,* vol. 798, p. Y8.6.1, 2004.

[6] K. Sato, P. H. Dederichs, H. Katayama-Yoshida, and J. Kudrnovsky, "Magnetic impurities and materials design for semiconductor spintronics," *Physica B,* vol. 340-342, pp. 863-869, 2003.

[7] I. T. Yoon, C. S. Park, H. J. Kim, Y. G. Kim, T. W. Kang, M. C. Jeong, M. H. Ham, and J. M. Myoung, "Characterization of ferromagnetic GaMnN layers grown on sapphire (0001) substrates," *Journal of Applied Physics,* vol. 95, pp. 591-596, 2004.

[8] A. Y. Polyakov, N. B. Smirnov, A. V. Govorkov, N. Y. Pashkova, J. Kim, F. Ren, M. E. Overberg, G. T. Thaler, C. R. Abernathy, S. J. Pearton, and R. G. Wilson, "Electrical and optical properties of GaN films implanted with Mn and Co," *Journal of Applied Physics,* vol. 92, pp. 3130-3135, 15 Sep 02 2002.

[9] B. Monemar, "Basic III-V research - Past, Present, and Future," *Journal of Crystal Growth,* vol. 189, pp. 1-7, 1998.

[10] T. Graf, M. Gjukic, M. S. Brandt, M. Stutzmann, and O. Ambacher, "The Mn[sup 3+/2+] acceptor level in group III nitrides," *Applied Physics Letters,* vol. 81, p. 5159, 2002.

[11] W. Limmer, W. Ritter, R. Sauer, B. Mensching, C. Liu, and R. Rauschenbach, "Raman Scattering in ion-implanted GaN," *Applied Physics Letters,* vol. 72, pp. 2589-2591, 1998.

[12] W. Gebicki, J. Strzeszewski, G. Kamler, T. Szyszko, and S. Podsiadlo, "Raman scattering study of Ga1-xMnxN crystals," *Applied Physics Letters,* vol. 76, pp. 3870-3872, 26 Jun 00 2000.

[13] H. Harima, "Raman studies on spintronics materials based on wide bandgap semiconductors," *Journal of Physics: Condensed Matter,* vol. 16, pp. S5653-S5660, 2004.

[14] M. Zajac, R. Doradzinski, J. Gosk, J. Szczytko, M. Lefeld-Sosnowska, M. Kaminska, A. Twardowski, M. Palczewska, E. Grzanka, and W. Gebicki, "Magnetic and optical properties of GaMnN magnetic semiconductor," *Applied Physics Letters,* vol. 78, pp. 1276-1278, 26 Feb 01 2001.

[15] M. Strassburg, J. Senawirante, C. Hums, N. Dietz, M. H. Kane, A. Asghar, A. M. Payne, I. T. Ferguson, C. J. Summers, U. Haboeck, A. Hoffman, D. Azamat, and W. Gelhoff,

"Optical and Structural Investigations on Mn-Ion States in MOCVD-grown Ga1-xMnxN," *MRS Proceedings,* vol. 831, p. E9.5.1, 2005.

[16] C. G. van de Walle and J. Neugebauer, "First-principles calculations for defects and impurities: applications to III-nitrides," *Journal of Applied Physics,* vol. 95, pp. 3851-3879, 2004.

[17] M. H. Kane, A. Asghar, M. Strassburg, Q. Song, A. M. Payne, C. J. Summers, Z. J. Zhang, N. Dietz, and I. T. Ferguson, "Impact of Manganese incorporation on the structural and magnetic properties of MOCVD-grown Ga1-xMnxN," *Materials Research Society Proceedings,* vol. 831, p. E9.4.1, 2005.

[18] R. Q. Wu, G. W. Peng, L. Liu, Y. P. Feng, Z. G. Huang, and Q. Y. Wu, "Cu-doped GaN: A dilute magnetic semiconductor from first-principles study," *Applied Physics Letters,* vol. 89, p. 062505, 2006.

[19] A. Zunger, "Electronic Structure of 3d Transition=Atom Impurities in Semiconductors," in *Solid State Physics*. vol. 39, H. Ehrenreich and D. Turnbull, Eds. New York: Academic Press, 1986, p. 275.

[20] T. Graf, T. B. Goennenwein, and M. S. Brandt, "Prospects for carrier-mediated ferromagnetism in GaN," *Physica status solidi (b),* vol. 239, pp. 277-290, 2003.

[21] T. Dietl, H. Ohno, F. Matsukura, J. Cibert, and D. Ferrand, "Zener Model Description of Ferromagnetism in Zinc-Blende Magnetic Semiconductors," *Science,* vol. 287, pp. 1019-1022, 11 Feb 2000 2000.

[22] J. M. D. Coey, M. Venkatesan, and C. B. Fitzgerald, "Donor impurity band exchange in dilute ferromagnetic oxides," *Nature Materials,* vol. 4, pp. 173-179, Feb 2005.

[23] E. Kartheuser, "Van Vleck paramagnetism of chromium- and iron-doped II-VI semiconductors," *Physical Review B (Condensed Matter and Materials Physics),* vol. 48, p. 14127, 1993.

[24] H. Przybylinska, A. Bonanni, A. Wolos, M. Kiecana, M. Sawicki, T. Dietl, H. Malissa, C. Simbrunner, M. Wegscheider, H. Sitter, K. Rumpf, P. Granitzer, H. Krenn, and W. Jantsch, "Magnetic properties of a new spintronic material-GaN:Fe," *Materials Science & Engineering B (Solid-State Materials for Advanced Technology),* vol. 126, pp. 222-5, 2006.

[25] S. Tanaka, M. Takeuchi, and Y. Aoyagi, "Anti-surfactant in III-nitride epitaxy - quantum dot formation and dislocation termination," *Japanese Journal of Applied Physics, Part 2: Letters,* vol. 39, pp. 831-834, 2000.

[26] T. Fukushima, K. Sato, H. Katayama-Yoshida, and P. H. Dederichs, "Spinodal decomposition under layer by layer growth condition and high curie temperature quasi-one-dimensional nano-structure in dilute magnetic semiconductors," *Japanese Journal of Applied Physics, Part 2: Letters,* vol. 45, pp. 416-418, 2006.

[27] M. H. Kane, S. Gupta, W. E. Fenwick, N. Li, E.-H. Park, M. Strassburg, and I. T. Ferguson, "Comparative study of Mn and Fe incorporation into GaN by metalorganic chemical vapor deposition," *Physica status solidi (b),* p. submitted, 2006.

[28] T. Dietl, "Self-organized growth controlled by charge states of magnetic impurities," *Nature Materials,* vol. 9, p. 673, 2006.

[29] F. Widmann, B. Daudin, G. Feuillet, Y. Samson, J. L. Rouviere, and N. T. Pelekanos, "Growth Kinetics and optical properties of self-organized GaN quantum dots.," *J. Appl. Phys.,* vol. 83, pp. 7618-7624, 1998.

[30] M. Miyamura, K. Tachibana, and Y. Arakawa, "High-density and size-controlled GaN self-assembled quantum dots grown by Metalorganic chemical vapor deposition," *Appl. Phys. Lett.,* vol. 80, pp. 3937-3939, 2002.

[31] N. Gogneau, D. Jalabert, E. Monroy, T. Shibata, S. Tanaka, and B. Daudin, "Stucture of GaN quantum dots grown under "modified Stranski-krastanow"conditions on AlN," *J. Appl. Phys.,* vol. 94, pp. 2254-2260, 2003.

[32] S. Gupta, H. Kang, M. Strassburg, A. Asghar, M. H. Kane, W. E. Fenwick, N. Dietz, and I. T. Ferguson, "A nucleation study of group III-nitride multifunctional nanostructures," *Journal of Crystal Growth,* 2005.

[33] P. Kratzert, M. Rabe, and F. Henneberger, "Self-Organized Formation of Wide-Bandgap II-VI Quantum dots. Thermally Activated surface Re-Organization versus 2D Stabilization," *Phys. Stat. sol.(b),* vol. 224, pp. 179-183, 2001.

[34] F. M. Ross, R. M. Tromp, and M. C. Reuter, "Transition states between pyramids and domes during Ge/Si island growth," *Science,* vol. 286, pp. 1931-1934, 1999.

[35] F. Widmann, J. Simon, N. T. Pelekanos, B. Daudin, G. Feuillet, J. L. Rouviere, and G. Fishman, "Giant piezoelectric effect in GaN self-assembled quantum dots," *Microelectronics Journal,* vol. 30, pp. 353-356, 1999 1999

[36] M. H. Kane, A. Asghar, C. R. Vestal, M. Strassburg, J. Senawiratne, Z. J. Zhang, N. Dietz, C. J. Summers, and I. T. Ferguson, "Magnetic and optical properites of $Ga_{1-x}Mn_xN$ grown by metalorganic chemical vapour deposition," *Semicond.Sci.Technol.,* vol. 20, p. L5, 2005.

[37] S. Kuroda, E. Bellet-Amalric, X. Biquard, J. Cibert, R. Giraud, S. Marcet, and H. Mariette, "Optimization of the growth of GaMnN epilayers using plasma-assisted MBE," *Phys. Stat. sol. (b),* vol. 240, pp. 443-446, 2003.

[38] A. L. Rosa, J. Neugebauer, J. E. Northrup, C.-D. Lee, and R. M. Feenstra, "Adsorption and incorporation of silicon at GaN(0001) surfaces," *Applied Physics Letters,* vol. 80, pp. 2008-2010, 2002.

[39] M. Copel, M. C. Reuter, E. Kaxiras, and R. M. Tromp, "Surfactants in epitaxial growth," *Physical Review Letters,* vol. 63, pp. 632-5, 1989.

[40] S. J. Pearton, C. R. Abernathy, G. T. Thaler, R. M. Frazier, D. P. Norton, F. Ren, Y. D. Park, J. M. Zavada, I. A. Buyanova, W. M. Chen, and A. F. Hebard, "Wide bandgap GaN-based semiconductors for spintronics," *Journal of Physics: Condensed Matter,* vol. 16, pp. 209-45, 2004.

[41] K. Sato and H. Katayama-Yoshida, "First principles materials design for semiconductor spintronics," *Semiconductor Science and Technology,* vol. 17, pp. 367-76, 2002.